A Novel Multi-band CO-OFDM based Long Reach Passive Optical Network Architecture

by

Mohamed Ben Zeglam

A thesis
presented to the University of Waterloo
in fulfillment of the
thesis requirement for the degree of
Master of Applied Science
in
Electrical and Computer Engineering

Waterloo, Ontario, Canada, 2017

© Mohamed Ben Zeglam 2017

I hereby declare that I am the sole author of this thesis. This is a true copy of the thesis, including any required final revisions, as accepted by my examiners.

I understand that my thesis may be made electronically available to the public.

Abstract

The thesis investigates a new long-reach passive optical networks (LRPON) architecture based on multi-band coherent optical orthogonal frequency division multiplexing (CO-OFDM). The proposed CO-OFDM based LRPON system is characterized by a novel phase noise compensation mechanism aiming to deal with optical signal dispersion in long-range transmissions. By employing a dispersion compensating fiber (DCF) and local oscillator (LO) laser phase shifter for each end-to-end transmission between OLT and ONU, we will show the phase noise due to dispersion can be effectively mitigated. Simulation of the downlink traffic between one optical line terminal (OLT) and 12 optical network units (ONUs) is performed successfully at different fiber lengths, at the data rate of $10Gbps$ per ONU. The required BER for the forward error correction (FEC) has been achieved for most ONUs, using a dispersion compensating fiber (DCF) and local oscillator (LO) laser phase shifter to compensate for the chromatic dispersion (CD) and the polarization mode dispersion (PMD), respectively.

Acknowledgements

All praise is to Allah for giving me the ability and knowledge to accomplish this thesis.

I would like to extend my gratitude to my supervisor, Professor Pin Han Ho, for offering me the opportunity to be a graduate student at the University of Waterloo, and for his continued support and guidance throughout my research.

I would like also to acknowledge the Libyan Ministry of Higher Education and Scientific Research for financially supporting this research work.

Thanks to all the my friends and UW staff members who helped me directly or indirectly during the course of my studies.

Dedication

I would like to dedicate this thesis to my parents, who started and nurtured my academic interests; to my beloved wife and my sons, who gave me the ultimate desire to finish this work; and to my brothers and sister, who support and encourage me all the time.

Table of Contents

List of Tables **ix**

List of Figures **x**

1 Introduction **1**

1.1 Background and Motivation 1

1.2 Contributions 3

1.3 Thesis Organization 4

2 Principles of OFDM **5**

2.1 OFDM Background 5

2.2 OFDM System 7

2.2.1 OFDM transmitters 9

2.2.2 OFDM Receiver 17

3 Optical OFDM System **19**

3.1 Optical OFDM Transmitter System 19

3.1.1 Intensity Modulation 21

3.1.2 Optical IQ modulator 23

3.2 Optical OFDM Receiver System 25

3.2.1 Direct Detection 25

3.2.2 Coherent Optical Detection 26

4 System Performance of Single-Band CO-OFDM for Different RF Frequencies **29**

4.1 Considered Single-Band CO-OFDM Transmission System 30

4.2 Evaluating the system with different subcarriers positions 34

4.2.1 The 64 subcarriers located between the 225^{th} and 288^{th} IFFT points 34

4.2.2 Relocating the 64-subcarriers to different position 36

4.3 Evaluating the system with phase dispersion compensation 41

4.3.1 Compensate phase dispersion by using DCF and initial phase shift . 42

4.4 Summary 44

5 System Performance of a Multi-band CO-OFDM Based LRPON **45**

5.1 Proposed Multi-band CO-OFDM PON Architecture 46

5.2 Simulation Setup and result 48

5.3 Summary 57

6 Conclusion and Future Work **58**

6.1 Conclusions 58

6.2 Future Work 59

References **61**

List of Tables

2.1 I/Q components for 16-QAM 12

4.1 System parameters 32

4.2 Initial phase for each 64-subcarrier location 42

5.1 The properties of the Sub-bands 49

List of Figures

1.1 Multi-band O-OFDM LRPON architecture 2

2.1 History of the evolution and implementation of OFDM [1] 6

2.2 The difference between FDM and OFDM spectrum 8

2.3 Block diagram of an OFDM transmitter 9

2.4 Different types of PSK constellation diagrams 10

2.5 Different types of QAM constellation diagrams 11

2.6 8-point DFT using decimation-in-time FFT algorithm 15

2.7 OFDM symbol with CP in time domain 16

2.8 Block diagram of an OFDM Receiver 18

3.1 Optical OFDM transmitter block diagram 20

3.2 O-OFDM transmitter based on intinsity modulator 22

3.3 Optical field and power transfer function of LN-MZM 23

3.4 O-OFDM transmitter based on optical IQ modulator 24

3.5 Optical OFDM receiver based on direct detection 26

3.6 Optical OFDM receiver based on direct detection 27

4.1 Architecture of single-band CO-OFDM system 31

4.2 OFDM symbol period 33

4.3 RF and optical OFDM power transmitting and receiving spectrum and constellation diagram for subcarriers located between the 225^{th} and 288^{th}. . . 36

4.4 RF OFDM transmitting power spectrum 37

4.5 CO OFDM transmitting power spectrum 38

4.6 CO OFDM receiving power spectrum 39

4.7 RF-OFDM receiving power spectrum 39

4.8 16-QAM constellation diagram for output of OFDM demodulator 40

4.9 The relationship of the $\log(BER)$ and Subcarrier position 40

4.10 16-QAM constellation diagram for the designed system with/without phase dispersion compensator 43

4.11 The relationship between the BER and transmitting power 44

5.1 Proposed Multi-band CO-OFDM PON Architecture 46

5.2 Assigning Subcarriers for Multi-band OFDM 48

5.3 Multi-band OFDM spectrum 51

5.4 Measured BER for the proposed multi-band CO-OFDM PON architecture compared with conventional CO-OFDM 52

5.5 16QAM and 16PSK constellation diagram for some sub-bands 53

5.6 The BRE at CW laser launched power -6dBm against transmission fiber length 55

5.7 The BRE at CW laser launched power -2dBm against transmission fiber length 56

Chapter 1

Introduction

1.1 Background and Motivation

In recent years, traffic in access networks has been increasing exponentially due to new services that have become available to subscribers, such as high definition TV, video call, on-line gaming, high speed internet, backbone mobile networks and cloud networks. As result of this rapid rise in traffic, optical passive networks (PON) are increasingly seen as promising architecture for access networks that could supply a high data-rate to subscribers economically.

Optical-OFDM based long-reach PON (O-OFDM LRPON) is one approach NG-PONs, and has attracted extensive attention from both academia and carrier operators due to its high data rate, long transmission distance, high spectral efficiency, and high power splitter ratios [2, 3]. It also demonstrates superb flexibility to allow real-time spectrum allocation

according to instantaneous service requirements [3]. Fig. 1.1 illustrates the multi-band O-OFDM LRPON of interest in this study. The OLT generates a multi-band O-OFDM signal for all ONUs that are launched in the transmission line. Following the power splitter, each ONU can identify its own sub-bands by synchronizing the subcarrier location assigned to it.

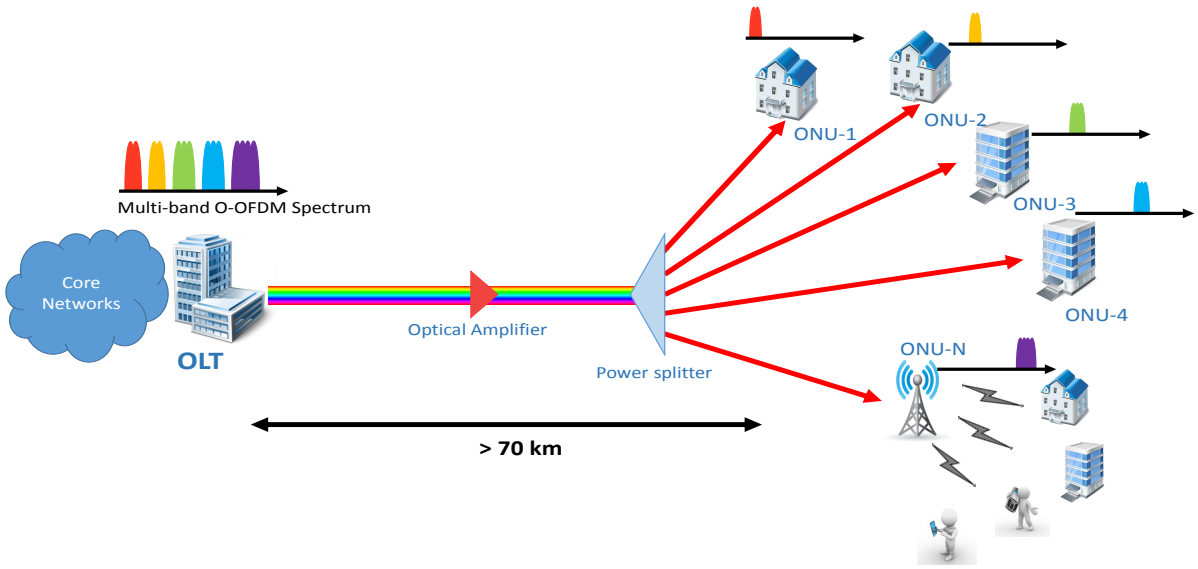

Figure 1.1: Multi-band O-OFDM LRPON architecture

There are two types of optical OFDM based PONs, classified according to the detection scheme, namely direct detection (DD) OFDM PON and coherent optical detection (CO) OFDM PON. Compared with DD-OFDM PON [3–7], only limited research exists on the CO-OFDM PON technique. In [8], eight wavelengths of WDM-ROF-PON based on 4QAM-OFDM technology have been achieved with 10 *Gbps* for each wavelength, to serve up to

64 users with $155Mbps/2.5Gbps$ guaranteed/peak rates. The authors in [9] discuss the received power sensitivity for four-band OFDM PONs under various fiber lengths. Note that the sub-bands generated by the multi-band CO-OFDM technology, although having a high data rate and long transmission distance, can be severely affected by chromatic dispersion (CD) and polarization mode dispersion (PMD). Moreover, the sub-bands that have high frequency are also severely affected by CD and PMD. Accordingly, several studies have suggested use of training-symbol and pilot-subcarrier techniques in the course of channel estimation so as to compensate for chromatic and polarization mode dispersions [3, 8, 9]. Nonetheless, this introduces overhead that decreases the transmission data rate. This issue has motivated the research described in this thesis on ways to compensate for CD and PMD without increasing the header on the transmission data rate.

1.2 Contributions

Based on the issues addressed in the previous section, The contributions of this thesis are as in the following:

- Propose a single-band CO-OFDM point-to-point transmission system, where we examine and improve its performance with different RF frequencies by compensating the phase noice due to CD and PMD.

- Propose a novel multi-band CO-OFDM based LRPON architecture that overcomes the malicious effect of phase noises by employing dispersion compensating fiber (DCF) and phase shift in LO laser at the receiver side for phase-noise elimination.

- Perform extensive simulate on the proposed multi-band CO-OFDM LRPON system, where we show that the CD and PMD can be well compensated for by employing DCF and phase shift in an LO laser, and the resultant BER performance can be significantly improved under all considered fiber lengths. We also compare the proposed system with two other legacy approaches: plain CO-OFDM without DCF and LO phase shift implemented, and conventional CO-OFDM where only DCF is used.

1.3 Thesis Organization

This thesis is organized as follows: Chapter 2 provides background information and illustrates the principle design of an OFDM transmitter and receiver. Chapter 3 provides the concept of incorporating an optical and an OFDM systems, and illustrates optical modulation and demodulation techniques. Chapter 4 examines the performance of a single-band CO-OFDM transmission system with the proposed phase compensation approach. Chapter 5 presents our design of a multi-band CO-OFDM based LRPON and its simulation results. Finally, the conclusion and future work are given in Chapter 6.

Chapter 2

Principles of OFDM

2.1 OFDM Background

OFDM has been used for a long time in wire and wireless telecommunication systems. In the 1870s, frequency division multiplexing (FDM) was used to send telegraph information over multiple channels [10]. Later on, orthogonal FDM was proposed to improve spectrum efficiency by overlapping multiple channels and avoiding the effect of intersymbol and interchannel interference [11]. Since then, researchers and developers in the field of telecommunications have investigated OFDM over the years and have managed to implement it in many applications. Fig. 2.1 shows a Discreet Fourier Transform was proposed in 1969 by Salz to create orthogonal signals [12]. In 1980, a cyclic extension, which today is known as the cyclic prefix, was used by Peled to eliminate ICI and ISI [13]. The developments described in this paragraph characterize the most basic OFDM system.

In the late twentieth century, researchers in wireless communication began to focus on how OFDM could be used in wireless applications. In 1985, an OFDM was proposed for

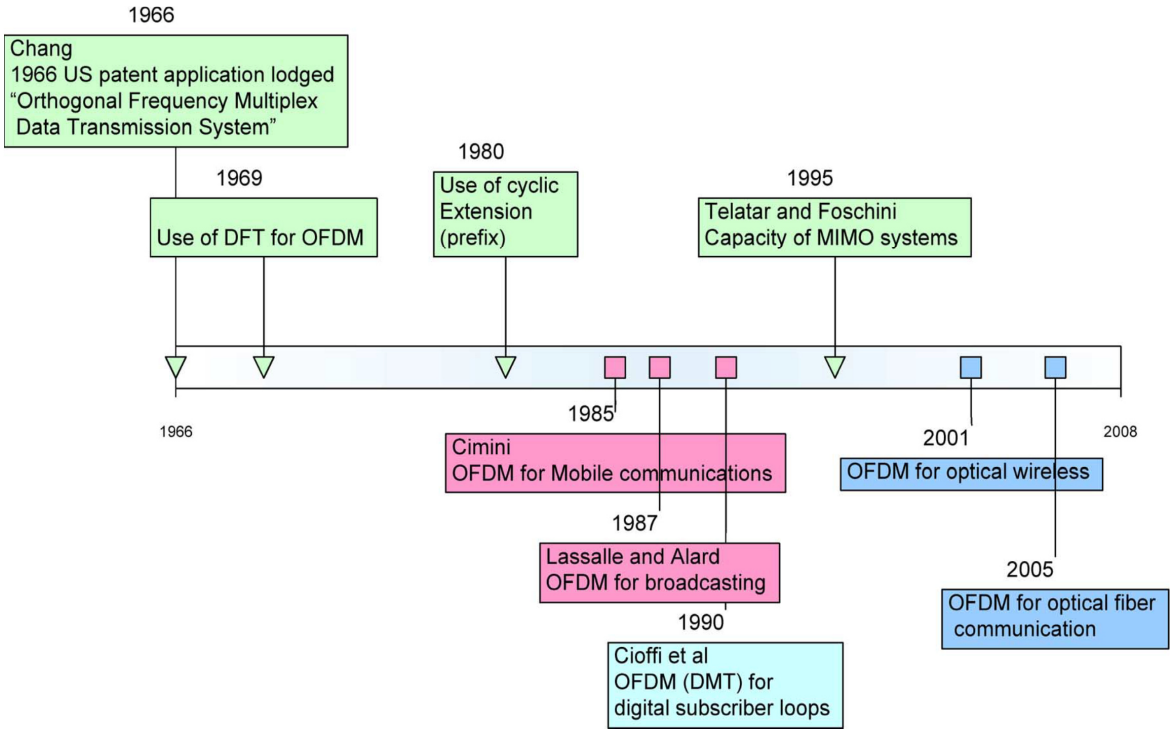

Figure 2.1: History of the evolution and implementation of OFDM [1]

mobile communications [14], and in 1987, a radio broadcast in France used OFDM technique to broadcast radio channels [15]. Many standards that use OFDM as a modulation

format have been issued, such as, IEEE 802.16e for WiMAX and IEEE 802.3 a/g for WiFi. In addition to wire line communications, a variation of OFDM called discrete multi tone (DMT) used for digital subscriber loops (DSL)was introduced in 1990 [16], and ITU issued standard ITU G.992.1 for ADSL technique.

In the twenty-first century, researchers started to investigate using OFDM in optical communication systems. Many experiments have been conducted recently on optical wireless [17]- [18] and fiber optic [2]- [19] systems. Optical OFDM is discussed in more detail in Chapter 3.

2.2 OFDM System

OFDM is a special case of FDM, as shown in Fig. 2.2. In FDM, different data is transmitted over a number of channels, and each channel has a different frequency carrier. A wide guard band is set between adjacent channels to prevent overlapping. This wide guard band makes the frequency spectrum inefficient, whereas in OFDM, the data is transmitted through multiple orthogonal channels. The advantage of OFDM is that the frequency spectrum is improved, even though channels are overlapping, by using inverse fast Fourier transform (IFFT) and FFT to modulate and demodulate the data respectively.

This section illustrates a standard OFDM system for wireless applications. OFDM systems have two main parts: the OFDM transmitter and receiver. Each has a number of

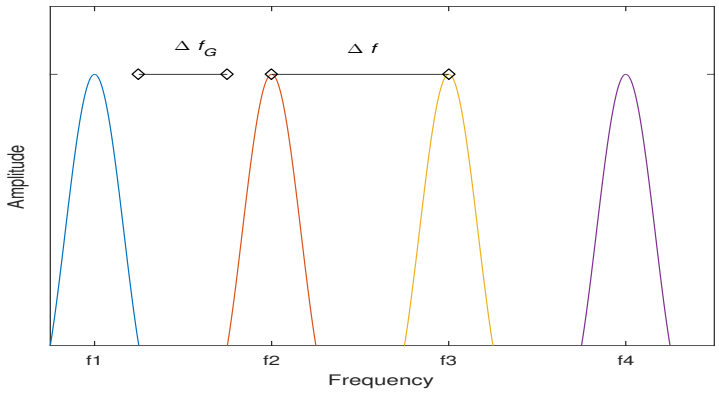

(a) FDM frequency spectrum

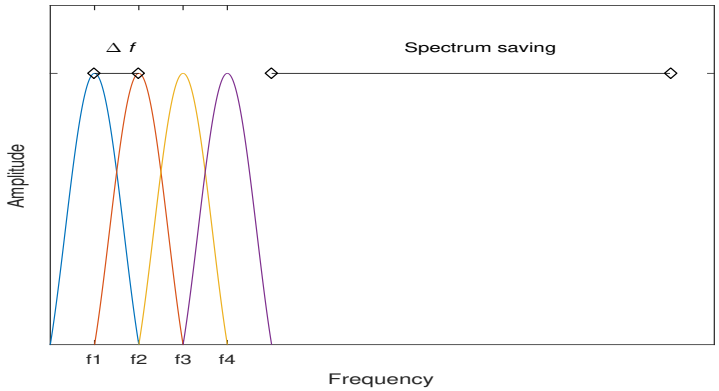

(b) OFDM frequency spectrum

Figure 2.2: The difference between FDM and OFDM spectrum

modules. The functionality and process of each module will be described in detail in the next subsections.

2.2.1 OFDM transmitters

In an OFDM transmitter, the input data, composed of serial bits, are first mapped to an M-array sequence generator followed by a serial-to-parallel converter; then an IFFT module is used to modulate each symbol to a certain subcarrier; afterwards a CP is added, followed by parallel-to-serial and digital-to-analog converters, as shown in Fig. 2.3 After all these processes, an OFDM signal is generated and ready to transmit over the channel.

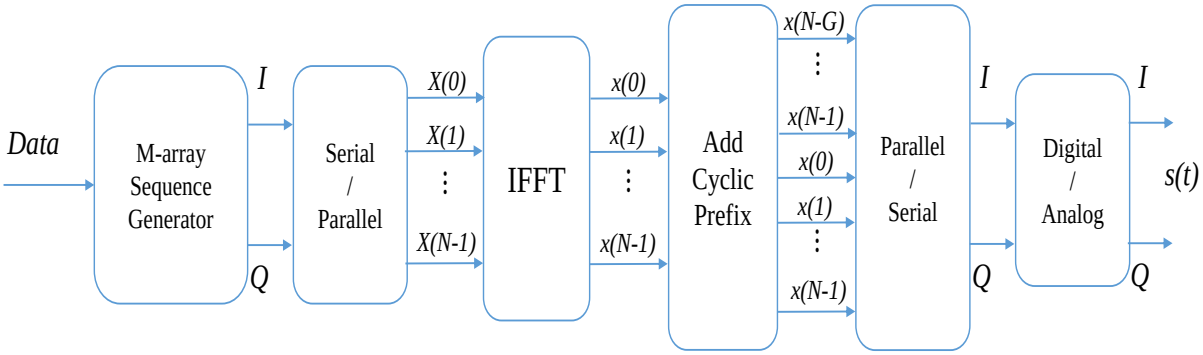

Figure 2.3: Block diagram of an OFDM transmitter

M-array Sequence Generator

The M-array sequence generator is used to code the bit sequence and split it into two parallel subsequences called the I/Q components. The coded format could be any of the digital modulation formats. The most common digital modulation used in OFDM systems are BPSK, QBSK, 8-PSK, 16-PSK, 4-QAM, 16-QAM and 64-QAM. The I and Q

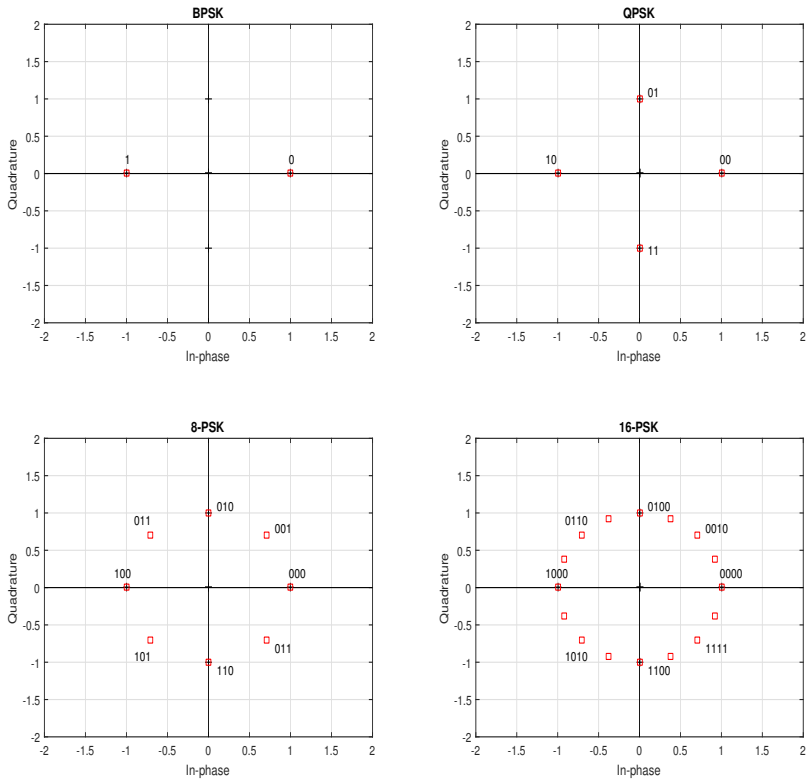

Figure 2.4: Different types of PSK constellation diagrams

components represent the x and y axes of a constellation diagram, respectively. Figs. 2.4 and 2.5 shown the different type of PSK and QAM constellation diagrams respectively. In a QAM sequence generator, the amplitude of each symbol changes according to Eq. 2.1

$$a_i = (2i - 1 - K), i = 1, 2, .., K \tag{2.1}$$

$$K = 2^{n/2} \tag{2.2}$$

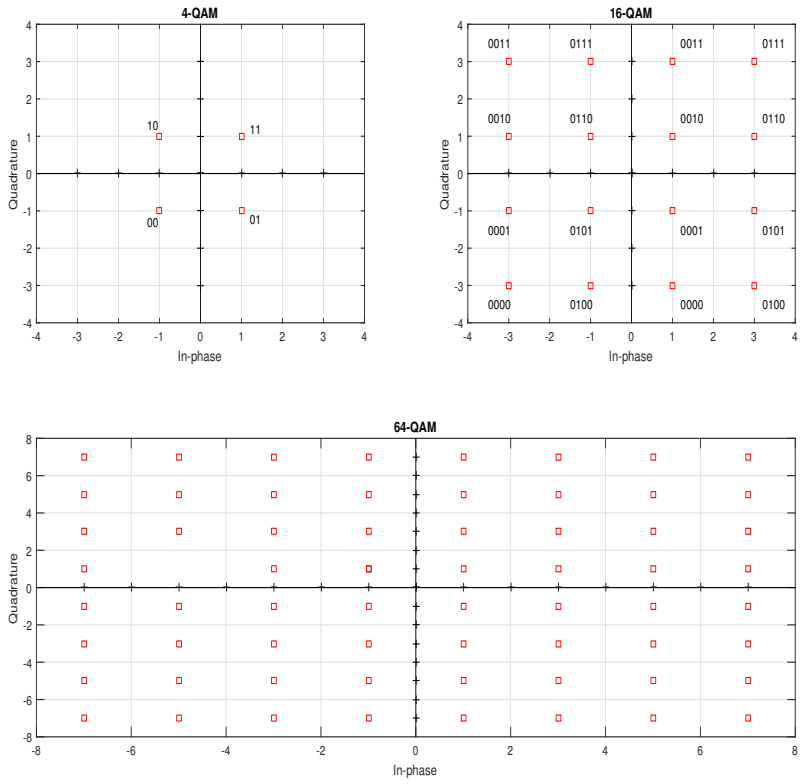

Figure 2.5: Different types of QAM constellation diagrams

where K is the number of possible sequences of binary digits, and n is the number of bits per symbol.

For example, in a 16-QAM, the number of bits per symbol is equal to four (n=4), and each two consecutive bits from the input sequence are mapped to one of the subsequences, which results in the number of possible sequences for each subsequence being equal to 4 (K=4). Table 2.1 shows that the amplitude depends on the symbols.

Table 2.1: I/Q components for 16-QAM

Sequence	In-phase (I)			Quadrature (Q)		
	Subsequence	i	a	Subsequence	i	a
0000	00	1	-3	00	1	-3
0001	00	1	-3	01	2	-1
0010	00	1	-3	10	3	1
0011	00	1	-3	11	4	3
0100	01	2	-1	00	1	-3
0101	01	2	-1	01	2	-1
0110	01	2	-1	10	3	1
0111	01	2	-1	11	4	3
1000	10	3	1	00	1	-3
1001	10	3	1	01	2	-1
1010	10	3	1	10	3	1
1011	10	3	1	11	4	3
1100	11	4	3	00	1	-3
1101	11	4	3	01	2	-1
1110	11	4	3	10	3	1
1111	11	4	3	11	4	3

Serial-to-Parallel and Parallel-to-serial conversion

For the serial-to-parallel conversion, the subsequence of I/Q components from the M-array sequence generator are split into N parts, where N is the number of subcarriers used to modulate the data to the OFDM signal. Each part has a sequence of symbols, and each symbol has a number of bits that depends on the digital modulation scheme. In contrast, the parallel-to-serial conversion is an inverse process, which combines N parts into I/Q components. N is the size of the IFFT.

IFFT

The IFFT is the main module in modern OFDM transmitters. It is a fast algorithm for computing inverse Discrete Fourier Transform (IDFT) [12]. The advantages of using IFFT in OFDM transmitters are that it is less complex than IDFT and can grantee the orthogonality between subcarriers [12] [20]. The function of IFFT is to convert a discrete frequency domain of the complex input sequence $X(m)$, mapped from an S/P converter, to the complex output sequence in the discrete time domain $x(n)$. Eq. 2.3 shows the general formula of IDFT.

$$x(n) = \frac{1}{N} \sum_{n=0}^{N-1} X(m) e^{\frac{j2\pi nm}{N}} \tag{2.3}$$

where $n = 1, 2, \ldots, N-1$, $m = 1, 2, \ldots, N-1$, and N is the IDFT poin. N is also known as the size of the IFFT. In another way, IDFT can be defined using the linear transformation between discrete time and frequency sequences, $x(n)$ and $X(m)$, respectively. Eq's. 2.4 and 2.5 show the N point vectors of $\mathbf{X_N}$ and $\mathbf{x_N}$, respectively, and Eq. 2.6 shows the $N \times N$ matrix of the linear transformation, $\mathbf{W_N}$ [21]

$$\mathbf{X_N} = [X(0), X(1), .., X(N-1)]^T \tag{2.4}$$

$$\mathbf{x_N} = [x(0), x(1), .., x(N-1)]^T \tag{2.5}$$

$$\mathbf{W_N} = \begin{bmatrix} {W_N}^{00} & {W_N}^{01} & \cdots & {W_N}^{0(N-1)} \\ {W_N}^{10} & {W_N}^{11} & \cdots & {W_N}^{1(N-1)} \\ \vdots & \vdots & \ddots & \vdots \\ {W_N}^{(N-1)0} & {W_N}^{(N-1)1} & \cdots & {W_N}^{(N-1)^2} \end{bmatrix} \tag{2.6}$$

$$W_N = e^{\frac{j2\pi}{N}} \tag{2.7}$$

The formula of the IDFT is expressed in Eq. 2.8 using Eq's. 2.4, 2.5 and 2.6, where $\mathbf{W_N^*}$ is a complex conjugate of the matrix $\mathbf{W_N}$ [21]

$$\mathbf{x_N} = \frac{1}{N}\mathbf{W_N^*}\mathbf{X_N} \tag{2.8}$$

There are many algorithms of IFFT that can be used to compute IDFT. One of these algorithms is called the decimation-in-time algorithm. In this algorithm, the N point of the IDFT is divided into two parts, with each part having a length of $N/2$. The IDFT is then performed for each part. This process of dividing the point of IDFT to two parts is then repeated until IDFT is computed for one point [21]. This algorithm reduces the complicity from $O(N^2)$ to $O(N \log N)$. Fig. 2.6 shows the decimation-in-time FFT for eight points.

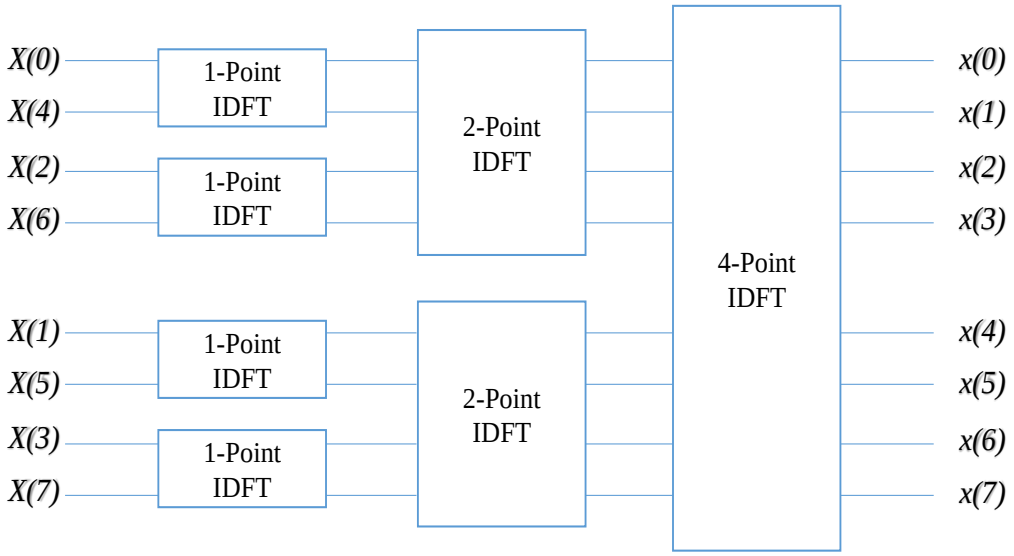

Figure 2.6: 8-point DFT using decimation-in-time FFT algorithm

Cyclic Prefix (CP)

This module extends the waveform of OFDM into a guard interval. As shown in Fig. 2.7 the end numbers of sampling from the OFDM symbol are copied into a guard interval in the beginning of the OFDM symbol. Therefore, the sequence shown in Eq. 2.9 is transmitted instead $\mathbf{x} = [x(0), x(1), .., x(N-1)]^T$ [1].

$$\mathbf{x}_{withCP} = [x(N-G), ..., x(N-1), x(0), x(1), .., x(N-1)]^T \tag{2.9}$$

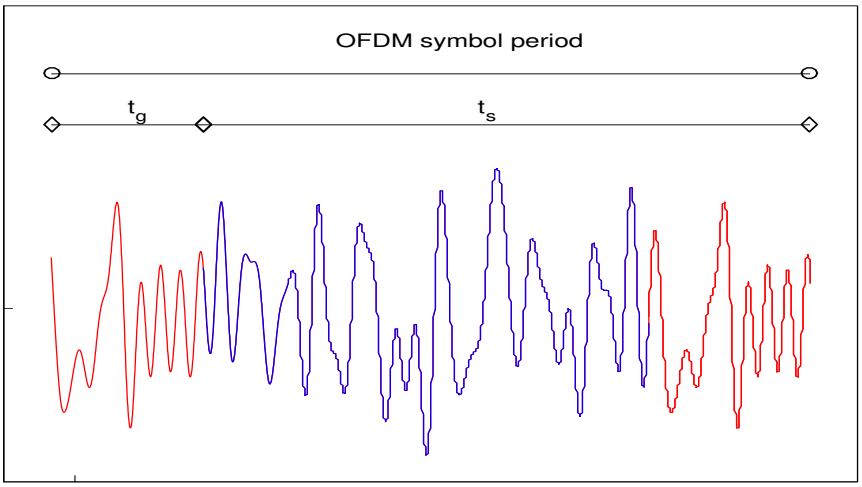

Figure 2.7: OFDM symbol with CP in time domain

where G is the size of the cyclic prefix. It is clearly shown that the cyclic prefix perfectly prevents both ICI and ISI from happening, if and only if the guard time interval Δ_G is greater than the maximum time delay spread [22]. However, CP increases the overhead, which reduces the transmitting data rate

$$R_b = \frac{nN_{sc}}{t_g + t_s} \tag{2.10}$$

where n is the number of bits per symbol, N_{sc} is the number of subcarriers, and t_s and t_g are the observation period, and guard time respectively. After the CP is added, P/S conversion is performed to convert the parallel sequence to a serial sequence.

Digital-to-Analog Converter

The serial output sequence of the P/S conversion is passed through a DAC, where the discrete time sequence is changed to continuous. The output of the DAC is given the base band OFDM signal, which can be expressed as [22]:

$$x(t) = \sum_{i=-\infty}^{\infty} \sum_{k=1}^{N_{sc}} c_{ki} e^{j2\pi f_k (t - iT_s)} f(t - iT_s) \tag{2.11}$$

$$f_k = \frac{k-1}{t_s}, \Delta f = \frac{1}{t_s} \tag{2.12}$$

$$f(t) = \left\{ \begin{array}{ll} 1, & (-\Delta_G < t \leq t_s) \\ 0, & (t \leq -\Delta_G, t > t_s) \end{array} \right\} \tag{2.13}$$

where C_{ki} is the information about the i^{th} symbol in subcarrier k^{th}, f_k is the subcarrier's frequency, Δf is the spacing between two adjacent subcarriers, and T_s is the OFDM symbol period with CP.

2.2.2 OFDM Receiver

At the receiver side, inverse processing of an OFDM transmitter is performed for the received signal. In Fig. 2.8 shows the receiving signal, which is defined as a cyclic convolution between the base band OFDM transmitted signal $s(t)$ and the impulse response of the transmitting channel $h(t)$, is passed through the ADC to digitalizing the signal. Then,

the ADC output is converted from a serial to a parallel sequence. After that, the CP is removed and passed to the FFT module, which de-modulates and de-multiplexes the signal. Finally, the signal is decoded using the M-array sequence decoder. Eq. 2.14 represents the

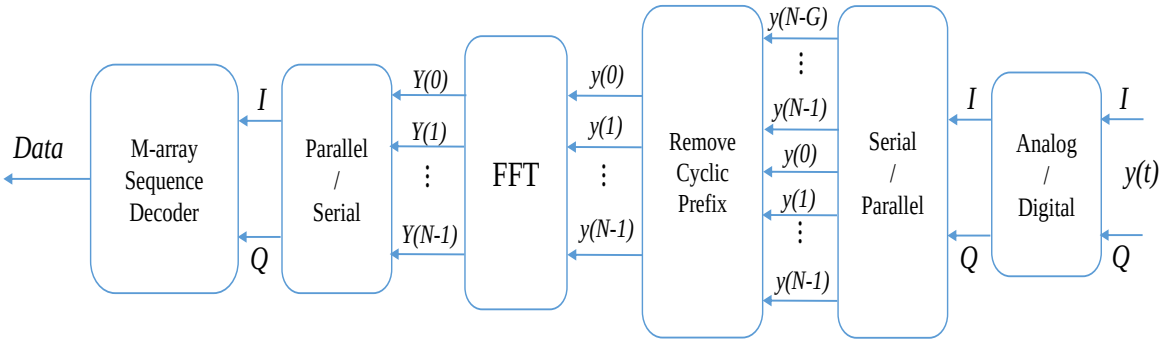

Figure 2.8: Block diagram of an OFDM Receiver

received signal, and Eq's. 2.15 and 2.16 represent the digitalization sequences before and after removing the CP. Eq's. 2.17 and 2.18 express the FFT linear transformation and the frequency domain sampling of the FFT output.

$$y(t) = x(t) \otimes h(t) \tag{2.14}$$

$$\mathbf{y}_{withCP} = [y(N-G), ..., y(N-1), y(0), y(1), .., y(N-1)]^T \tag{2.15}$$

$$\mathbf{y_N} = [y(0), y(1), .., y(N-1)]^T \tag{2.16}$$

$$\mathbf{Y_N} = \mathbf{W_N y_N} \tag{2.17}$$

$$\mathbf{Y_N} = [Y(0), Y(1), .., Y(N-1)]^T \tag{2.18}$$

Chapter 3

Optical OFDM System

The previous chapter illustrated the principle of conventional OFDM. Recently, OFDM has been used as an advanced modulation in optical communication systems, because its advantages, such as high spectral efficiency and dispersion resistance. There are two main techniques of an Optical OFDM, classified based on the detection scheme at the receiver. These techniques are direct-detection OFDM (DD-OFDM) and coherent-detection OFDM (CO-OFDM). In many papers, the CO-OFDM shows better spectral efficiency and receiver sensitivity [2, 20, 22–24]. However, CO-OFDM needs a local optical source at the receiver to generate a local optical carrier, so it is more complex and costly than DD-OFDM.

3.1 Optical OFDM Transmitter System

The optical OFDM transmitter (Fig. 3.1) consists of two main parts: a baseband OFDM generator and an optical-up-conversion. The former has been discussed in the previous

section, and we will focus on the latter. In an optical-up-conversion, the I and Q components of an OFDM generator's output are modulated to an optical domain via an external optical modulator and a continuous wave laser source. There are two types of external optical modulators commonly used for O-OFDM systems: Intensity modulators and optical IQ modulators. Both are discussed in detail later. For each type, the lithium niobate Mach-Zehnder modulator (LN-MZM) is widely used, because it provides low optical loss and better performance for high data rates, and it can be use for high radio-frequency signals [25, 26].

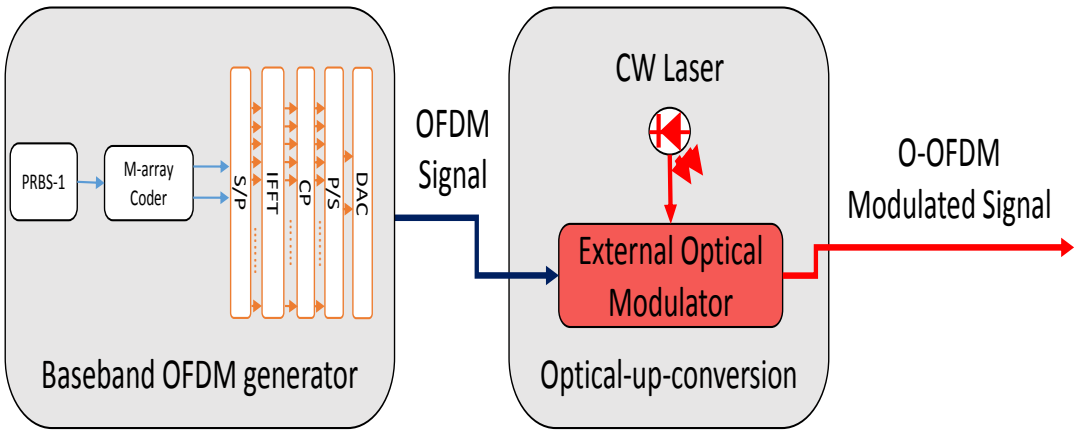

Figure 3.1: Optical OFDM transmitter block diagram

3.1.1 Intensity Modulation

The intensity modulator consists of a continuous wave laser and one LN-MZM. The output of the LN-MZM is directly proportional to the electrical-OFDM signal, and the E-OFDM must be a real and positive signal [27]. Therefore, the I and Q components of the OFDM generator's output, which represent the real and imaginary parts of a baseband OFDM signal, are converted to the real radio frequency OFDM signal by using an electrical IQ modulator, as shown in Fig 3.2. In LN-MZM, the input optical power, which comes from the CW laser, is split between two waveguide arms, and the electrical OFDM is applied to these two arms to enable optical phase modulation. The output of LN-MZM is the combination of two optical waves passing through two waveguide arms, The maximum intensity can be reached if the two arms are in-phase, resulting in constructive interference. [28].

The relation between the output optical field and the input optical field can be expressed as in Eq. 3.1, where $E_{out}(t)$ is the LN-MZM's output optical field, $E_{in}(t)$ is the LN-MZM's input optical field, ϕ_1 is the phase shift of the upper arm of LN-MZM, and ϕ_2 is the phase shift of the lower arm of LN-MZM. The phase shift can be represented by Eq. 3.2 [23].

$$E_{out}(t) = \frac{E_{in}(t)}{2} \cdot \left(e^{j\phi_1(t)} + e^{j\phi_2(t)}\right) \tag{3.1}$$

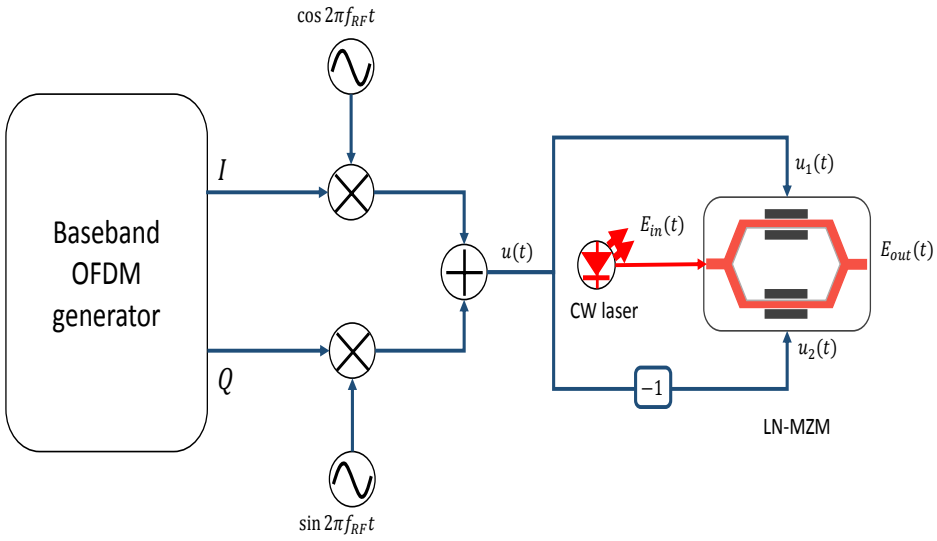

Figure 3.2: O-OFDM transmitter based on intinsity modulator

$$\phi_1 = \frac{\pi.u_1(t)}{V_\pi}, \phi_2 = \frac{\pi.u_2(t)}{V_\pi} \tag{3.2}$$

where $u_1(t)$ and $u_2(t)$ are the electrical OFDM signal on upper and lower electrodes, respectively. When the LN-MZM configuration is operating as a push-pull with $u_1(t) = -u_2(t) = u(t)/2$, then the LN-MZM's output electrical field and output power are written as in Eq. 3.3 and 3.4 [23], respectively. Fig. 3.3 shows the optical field and optical power transfer functions.

$$E_{out}(t) = E_{in}(t).\cos\left(\frac{\pi.u(t)}{2V_\pi}\right) \tag{3.3}$$

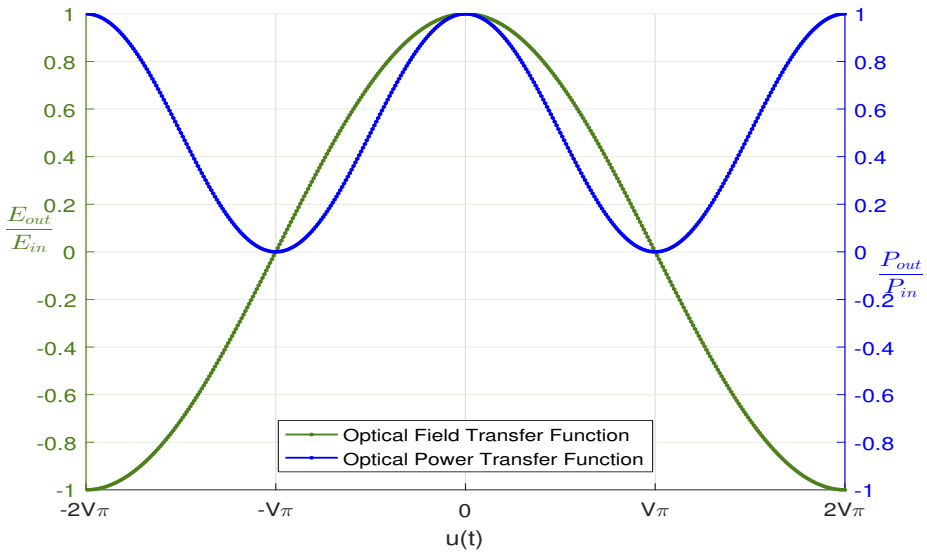

Figure 3.3: Optical field and power transfer function of LN-MZM

$$P_{out}(t) = P_{in}(t).\left(\frac{1}{2} + \frac{1}{2}\cos\left(\frac{\pi.u(t)}{V_\pi}\right)\right) \tag{3.4}$$

3.1.2 Optical IQ modulator

In Fig. 3.4, the I and Q components of the complex baseband OFDM signal are up-converted to the optical domain by an optical IQ modulator, which consists of a CW laser and and two LN-MZMs. The optical signal of the CW laser is connected to both LN-MZMs as an input optical signal for both LN-MZMs. The upper and bottom LN-MZMs modulate the input optical signal with the I and Q components of the baseband OFDM signal, respectively. In addition, both LN-MZMs are biased at null point in order to achieve

the linearity conversion. The output of the upper and bottom LN-MZMs can be expressed as in Eqs. 3.5 and 3.6 respectively [23].

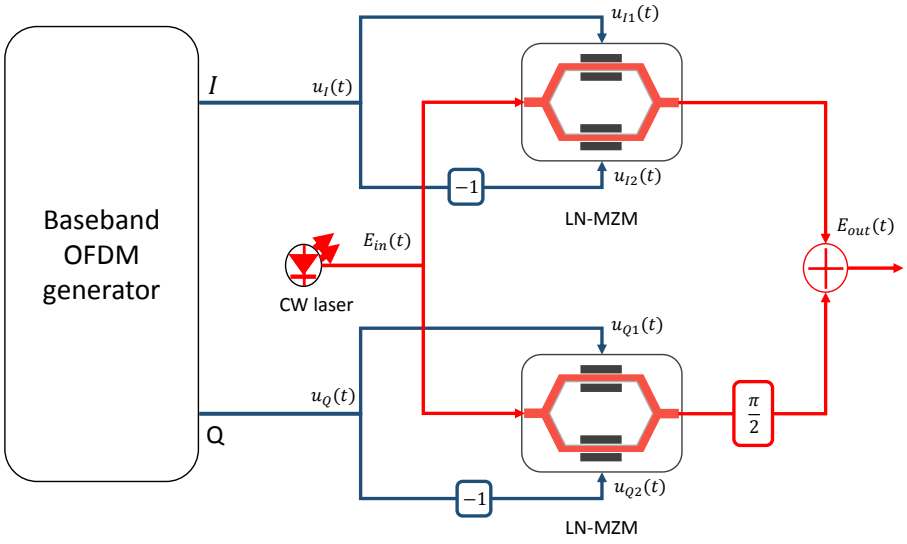

Figure 3.4: O-OFDM transmitter based on optical IQ modulator

$$E_{I-out}(t) = \frac{E_{in}}{2}.\cos\left(\frac{\pi}{2}\frac{u_I(t)}{V_\pi}\right) \tag{3.5}$$

$$E_{Q-out}(t) = \frac{E_{in}}{2}.\cos\left(\frac{\pi}{2}\frac{u_Q(t)}{V_\pi}\right) \tag{3.6}$$

The bottom LN-MZM's output is shifted by 90^o and then combined with output of the upper LN-MZM to generate an optical single side band OFDM (OSSB OFDM) signal. So the optical IQ modulator's output and transfer function can be written as in Eq. 3.7 and

3.8 [23].

$$E_{out}(t) = E_{I-out}(t) + E_{Q-out}(t).e^{\frac{j\pi}{2}}$$
$$E_{out}(t) = E_{I-out}(t) + jE_{Q-out}(t) \tag{3.7}$$

$$\frac{E_{out}(t)}{E_{in}} = \frac{1}{2}.\cos\left(\frac{\pi}{2}\frac{u_I(t)}{V_\pi}\right) + j\frac{1}{2}.\cos\left(\frac{\pi}{2}\frac{u_Q(t)}{V_\pi}\right) \tag{3.8}$$

3.2 Optical OFDM Receiver System

There are two types of optical detector in optical OFDM systems: direct-detection and coherent-detection. Direct-detection can be used when an intensity modulator is used at the transmitter side, whereas coherent-detection can be used when an optical IQ modulator is used at the transmitter side. Both types of optical detector convert received optical signals to a baseband OFDM signal, as discussed in detail in the next sub-sections. A baseband OFDM signal is passed to an OFDM demodulator, as discussed in detail in previous chapter in section 2.2.2. Coherent-detection has better receiver sensitivity than direct-detection, but it is more costly and complex.

3.2.1 Direct Detection

In direct-detection, the received optical signal, where an IM is used at the transmitter, is detected by a single photodiode, which converts the power of optical signals into electrical

current. After that, the electrical IQ demodulator is used to down-convert RF-OFDM to a baseband OFDM signal, which has both real and imaginary OFDM components as shown in Fig. 3.5. In IM-DD-OFDM systems, a guard-band is required between the OFDM band and an optical carrier; therefore, the electrical IQ (de)modulator should be working on high RF frequency. Thus, IM-DD-OFDM has less spectral efficiency. However, IM-DD-OFDM is considered to be a cost-effective solution due to the design simplicity of IM/DD systems.

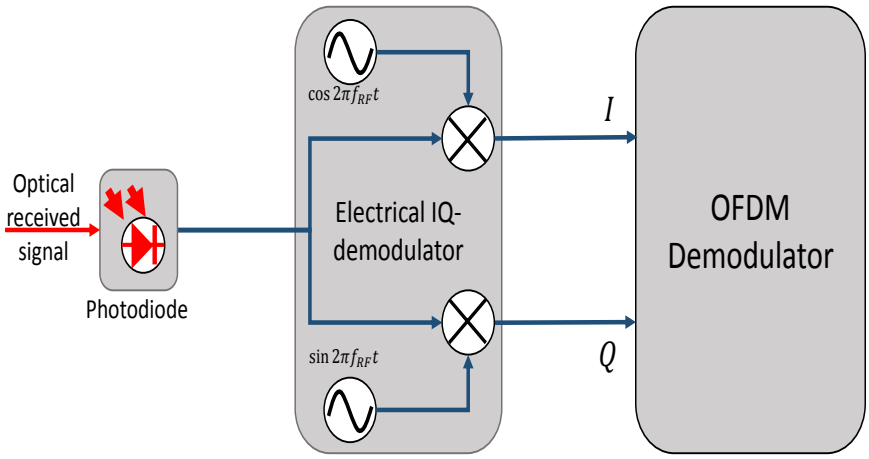

Figure 3.5: Optical OFDM receiver based on direct detection

3.2.2 Coherent Optical Detection

Coherent-optical detection is needed when an optical OFDM signal is modulated using an optical IQ modulator. As shown in Fig. 3.6, a coherent-optical detector consists of a local oscillator (LO), a 90^o optical hybrid, and two balanced photo detectors. The I and Q

components are recovered by down-converting the incoming O-OFDM signal with the LO signal linearly [23]. The 90^o optical hybrid generates phase shifts of 90^o and 180^o for the I/Q components and balanced detector, respectively. The four output signals of the 90^o optical hybrid can be written as in Eq. 3.9 [23].

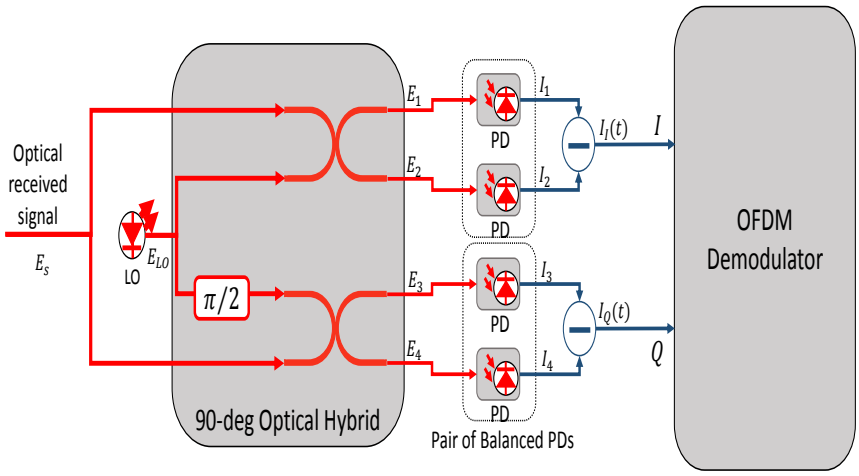

Figure 3.6: Optical OFDM receiver based on direct detection

$$E_1 = \frac{1}{\sqrt{2}}\left[E_s + E_{LO}\right], E_2 = \frac{1}{\sqrt{2}}\left[E_s - E_{LO}\right]$$
$$E_3 = \frac{1}{\sqrt{2}}\left[E_s + jE_{LO}\right], E_4 = \frac{1}{\sqrt{2}}\left[E_s - jE_{LO}\right] \tag{3.9}$$

where E_s is the received O-OFDM signal, and E_{LO} is the LO optical signal. Each of these outputs is detected by photodiode, which converts the optical power to electrical current. The output of each photodiode can be expressed as in Eq. 3.10, whereas a pair of balanced detectors' outputs are expressed in Eq. 3.11 [23].

$$
\begin{aligned}
I_1 &= |E_1|^2 = \frac{1}{2}\left\{|E_s|^2 + |E_{LO}|^2 + 2Re\left\{E_s E_{LO}^*\right\}\right\} \\
I_2 &= |E_2|^2 = \frac{1}{2}\left\{|E_s|^2 + |E_{LO}|^2 - 2Re\left\{E_s E_{LO}^*\right\}\right\} \\
I_3 &= |E_3|^2 = \frac{1}{2}\left\{|E_s|^2 - |E_{LO}|^2 + 2Im\left\{E_s E_{LO}^*\right\}\right\} \\
I_4 &= |E_4|^2 = \frac{1}{2}\left\{|E_s|^2 - |E_{LO}|^2 - 2Im\left\{E_s E_{LO}^*\right\}\right\}
\end{aligned}
\tag{3.10}
$$

$$
\begin{aligned}
I_I(t) &= I_1 - I_2 = 2Re\left\{E_s E_{LO}^*\right\} \\
I_Q(t) &= I_3 - I_4 = 2Im\left\{E_s E_{LO}^*\right\}
\end{aligned}
\tag{3.11}
$$

Chapter 4

System Performance of Single-Band CO-OFDM for Different RF Frequencies

In this chapter, a single-band CO-OFDM transmission system is designed and simulated using a commercial simulation tool called Optisystem V.14. The impacts of chromatic dispersion and polarization mode dispersion on different RF frequencies have been observed, followed by an investigation into how the system's performance can be improved by optimal power transmission and by compensating for both chromatic dispersion and polarization mode dispersion.

The structure of this chapter is as follows: it starts with a structural design for the single-band CO-OFDM system; then it describes simulating the system with different subcarrier positions to evaluate system performance; after that the system is modified and simulated with phase dispersion compensation.

4.1 Considered Single-Band CO-OFDM Transmission System

The single-band CO-OFDM has been designed using Optisystem simulation tool version 14. Fig. 4.1 shows the architecture of the single-band CO-OFDM system, which consists of a CO-OFDM transmitter, an optical channel, and a CO-OFDM receiver. In the CO-OFDM transmitter, a binary input sequence of 10 Gb/s is generated using Pseudo Random Binary Sequence (PRBS) and mapped to 16-QAM to generates two parallel M-array sequences. The output M-array signal of the 16-QAM is passed to an OFDM modulator with the following parameters: 512 IFFT points, 64 effective subcarriers, 50 dBm average OFDM power and 32 prefix points that add 1/16 of the OFDM symbol period with CP to the total baseband OFDM symbol period. The output of the OFDM modulator, which is defined as in-phase I and quadrature Q, is passed through the band-pass filter. The output is then up-converted to the optical domain using an RF-to-optical converter consisting of a laser source with a power of -6 dBm, two lithium Niobate Mach-Zehnder modulators (LiNB-MZM), and an optical amplifier with a gain of 20 dBm.

In an optical channel, an optical signal is transmitted over an SMF with a length of 84 km, an attenuation of 0.2 dBm/km, and a dispersion of 16 ps/nm/km. An optical amplifier is used to compensate for the lost of fiber attenuation. In the CO-OFDM receiver, optical received signals are detected by a coherent detector that down-converts optical signals

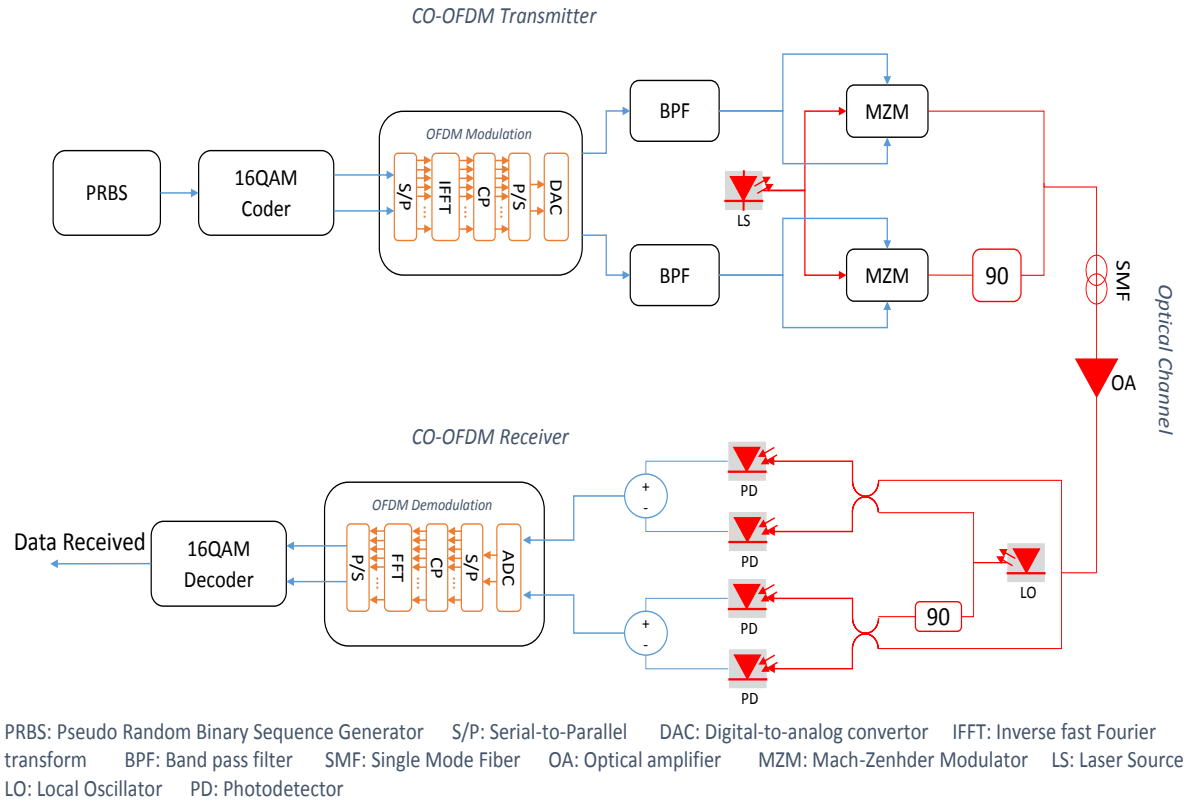

Figure 4.1: Architecture of single-band CO-OFDM system

to RF signals. The coherent detector consists of four PIN photo-diodes, each one with a dark current of 10 nA, and a local oscillator with a power of -5 dBm. After down-converting to RF signals, a demodulation is performed by the OFDM demodulator, whose its parameters are set with the same parameters as the OFDM modulator. The output of the OFDM demodulator is mapped to the 16-QAM decoder, which decodes the M-array sequence back into a binary sequence. Table 4.1 illustrates more details of the system

parameters.

Table 4.1: System parameters

Global Parameter	
Bit rate (R_b)	10 $Gbps$
Sequence length	131072 $bits$
Number of bit per symbol (n)	4
Symbol rate (R_s)	2.5 $Gsymbols/s$
OFDM Modulation/Demodulation Parameters	
(I)FFT points ($IFFT_p$)	512
Number of Subcarriers (N_{sc})	64
Prefix Point (Pr_p)	32
Average OFDM power	50 dBm
RF-to-optical up-converter Parameters	
Laser source power	-6 dBm
Optical carrier frequency (f_{LD})	193.1 THz
Initial phase	0°
Optical-to-RF down converter Parameters	
Local oscillator power	-5 dBm
Local oscillator frequency	193.1 THz
Local oscillator phase	0°
SMF Parameters	
Fiber length (L)	84 km
Attenuation	0.2 dB/km
Dispersion (D)	16 $ps/nm/km$
Differential Group Delay (DGD)	0.2 ps/km

The following equations explain how Optisystem computes some operation parameters, starting with the frequency spacing between adjacent subcarriers Δf, then the observation period t_s, CP operator η and period t_g, total OFDM period T_s, and net data transmission rate R_B.

$$\Delta f = \frac{R_s}{N_{sc}} = \frac{2.5 Gsymbols/s}{64} = 39.0625 MHz \tag{4.1}$$

$$t_s = \frac{1}{\Delta f} = \frac{1}{39.0625MHz} = 25.6ns \tag{4.2}$$

$$\eta = \frac{Pr_p}{FFT_p} = \frac{32}{512} = 1/16 \tag{4.3}$$

$$t_g = t_s \times \eta = 25.6ns \times \frac{1}{16} = 1.6ns \tag{4.4}$$

$$T_s = t_s + t_g = 25.6ns + 1.6ns = 27.2ns \tag{4.5}$$

$$R_B = \frac{n \times N_{sc}}{T_s} = \frac{4 \times 64}{27.2ns} = 9.412Gbps \tag{4.6}$$

$$IFFT_{bandwidth} = \frac{FFT_p \times \Delta f}{2} = \frac{512 \times 39.0625MHz}{2} = 10GHz \tag{4.7}$$

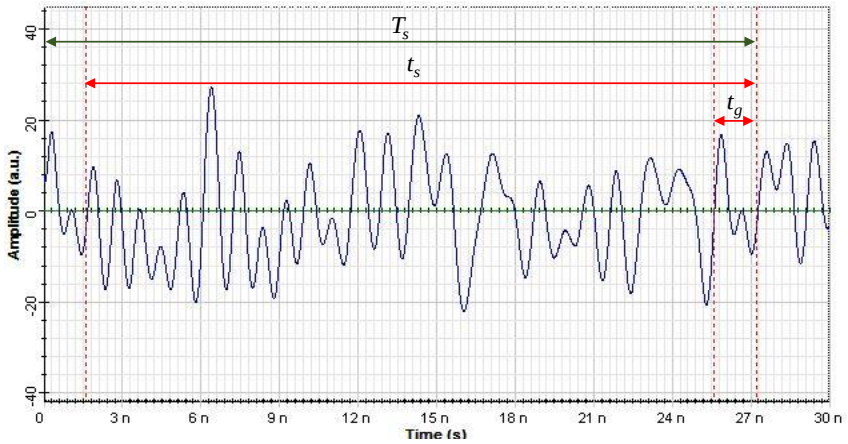

Figure 4.2: OFDM symbol period

Each point of the IFFT module at the OFDM modulator has a frequency, called the subcarrier frequency. The zero subcarrier frequency is located at the middle of the $IFFT_p$. In this case and as per Table 4.1, the 257^{th} subcarrier has zero Hz. The subcarriers on the left and right sides of the 257^{th} subcarrier have the same frequencies that can be obtained

using Eq. 4.8, where k is the location of the subcarrier at IFFT points and m is the integer number, which can be defined as in Eq. 4.9.

$$f_k = m\Delta f \tag{4.8}$$

$$m = \left| k - (\frac{IFFT_p}{2} + 1) \right| \tag{4.9}$$

However, the subcarriers located in the left side of zero frequency will up-convert to the optical domain on the left side of the optical carrier frequency, while the right side subcarriers will be on the right side of optical carrier frequency in the optical domain.

4.2 Evaluating the system with different subcarriers positions

A simulation has been performed for the designed system with the different band positions of the 64 subcarriers around the IFFT points. The BER is measured to evaluate system performance. In addition, the impacts of chromatic and polarization mode dispersion are observed. The position of the 64 subcarriers change as follows:

4.2.1 The 64 subcarriers located between the 225^{th} and 288^{th} IFFT points

The data is carried on 64 subcarriers located in the IFFT between the 225^{th} and 288^{th} points. This band is located exactly so that 32 subcarriers are on the left and 31 are on

the right side of zero frequency. Fig 4.3a shows the power spectrum of the transmitting base band OFDM signal in RF mode where the power is equal to $28dBm$, while Fig. 4.3b shows the CO-OFDM power spectrum, where the power is equal to $-32dBm$, and the optical carrier frequency ($193.1THz$) is in the middle of the CO-OFDM band. Fig. 4.3b also illustrates that subcarriers located on the left and right sides of the zero subcarrier are located in the left and right sides of the optical carrier frequency.

4.3 On the receiver side, the receiving optical power signal is equal to $-31.56dBm$, as shown in Fig. 4.3c, and is also the same as the transmission power, because the optical amplifier compensates for the fiber attenuation. The OSNR is equal to $30.6dB$, which is measured using an optical analyzer with a $0.0002nm$ bandwidth resolution. Fig. 4.3d presents the OFDM power spectrum for the output of coherent detection where the signal and noise power are equal to $-51.2dBm$ and $-96.5dBm$, respectively. The SNR at this stage is equal to $45.3dB$, and is measured using an electrical analyzer with a $10MHz$ bandwidth resolution. As an output of OFDM demodulation, the 16-QAM constellation diagram of $10Gbps$ is almost clear as shown in Fig.4.3e. After that, the 16-QAM decoder is used, and the BER is measured, the $\log(BER)$ was found to be -5.1. The location of the 64 subcarriers in this test shows good results in terms of the BRE.

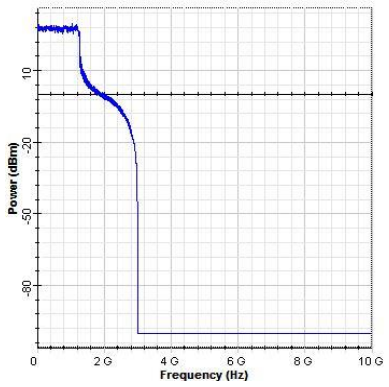

(a) RF OFDM transmitting power spectrum

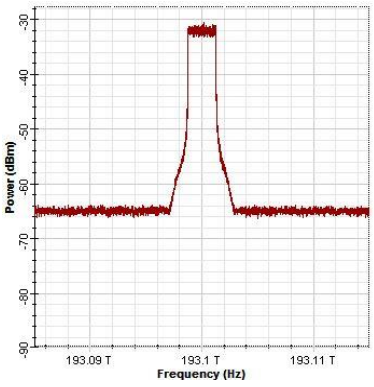

(b) Optical OFDM transmitting power spectrum

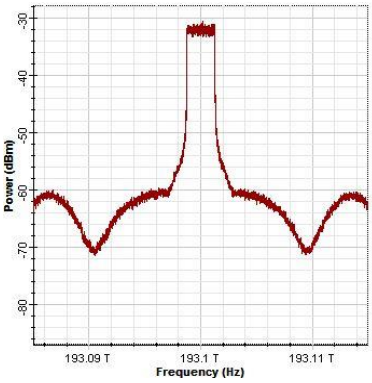

(c) Optical OFDM receiving power spectrum

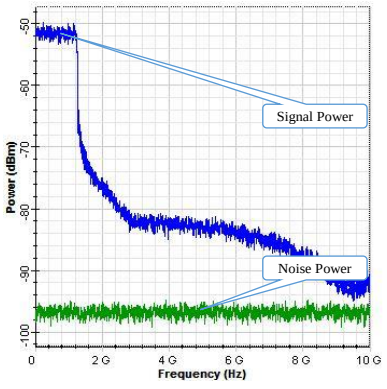

(d) RF OFDM receiving power spectrum

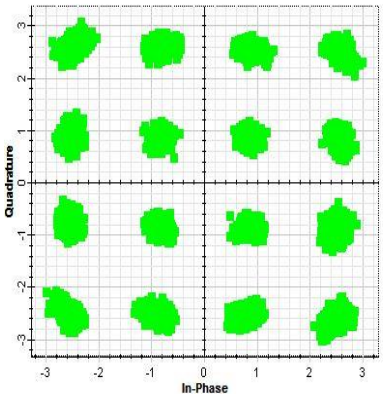

(e) 16-QAM constellation diagram at receiver side

Figure 4.3: RF and optical OFDM power transmitting and receiving spectrum and constellation diagram for subcarriers located between the 225^{th} and 288^{th}.

4.2.2 Relocating the 64-subcarriers to different position

Multiple iterations are performed to evaluate the system's performance by relocating the 64 subcarriers to different position along the IFFT module. The 64 subcarriers are relocated as follows: from point 104^{th} to 167^{th} in case one, from point 185^{th} to 248^{th}in case two,

from point 266^{th} to 329^{th} in case three, from point 347^{th} to 410^{th}in case four. Fig. 4.4 shows the power spectrum for the output of the OFDM modulator for the four cases; the RF-OFDM power is around $25dBm$. The electrical band frequency for the 64 subcarriers in cases two and three begins at $0.35GHz$ and ends at $2.81GHz$ as shown in Fig. 4.4b and 4.4c respectively, while in cases one and four it begins at $3.52GHz$ and ends at $5.98GHz$, as shown in Fig. 4.4a and 4.4d, respectively.

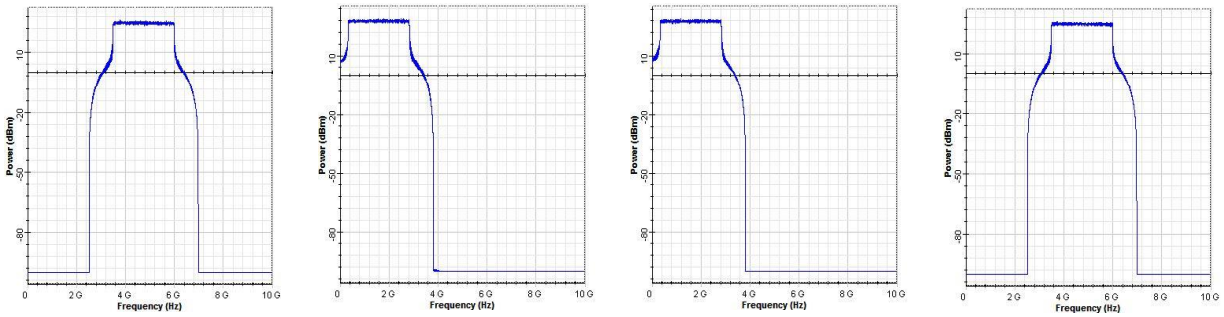

(a) Case one (b) Case two (c) Case three (d) Case four

Figure 4.4: RF OFDM transmitting power spectrum

After RF-to-optical up-conversion is performed, the CO-OFDM power spectrum is as shown in Fig. 4.5, and the power is approximately $-31.5dBm$ for all cases. Since the 64 subcarriers for cases one and two are located on the left side of the zero subcarrier frequency, Fig. 4.5a and 4.5b clearly show that these two cases are up-converted to the optical domain on the left side of the optical carrier frequency. In contrast, Fig. 4.5c and 4.5d clearly show that cases three and four are up-converted to the optical domain on the

right side of the optical carrier frequency since they are located on the right side of the zero subcarrier frequency.

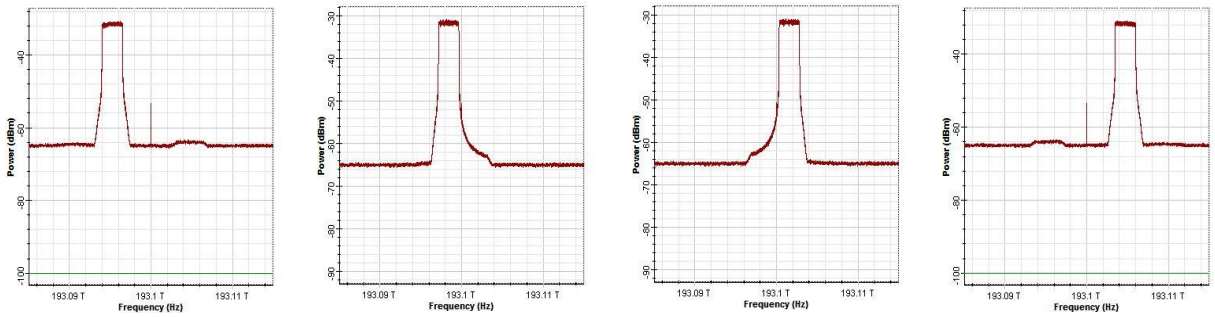

(a) Case one (b) Case two (c) Case three (d) Case four

Figure 4.5: CO OFDM transmitting power spectrum

At the receiver side, the CO-OFDM signal received is affected by the nonlinear impairments. Fig. 4.6 shows the CO-OFDM power spectrum for the receiving signal, where the power level is $-31dBm$, which is the same as power transmitted due to the fact that the fiber attenuation is compensated for by the optical amplifier. Fig. 4.7 shows the power spectrum for the coherent detection output, The signal power and noise power for all cases are almost $-53dBm$ and $-95dBm$, respectively. The OSNR and SNR for all cases are approximately $31.8dB$ and $42dB$, respectively.

OFDM demodulation and digital signal processing then taken place. A 16-QAM constellation diagram for $10Gbps$ of the single band CO-OFDM system, shown in Fig. 4.8, illustrates that there is a phase dispersion for each subcarrier. It is clearly shown that

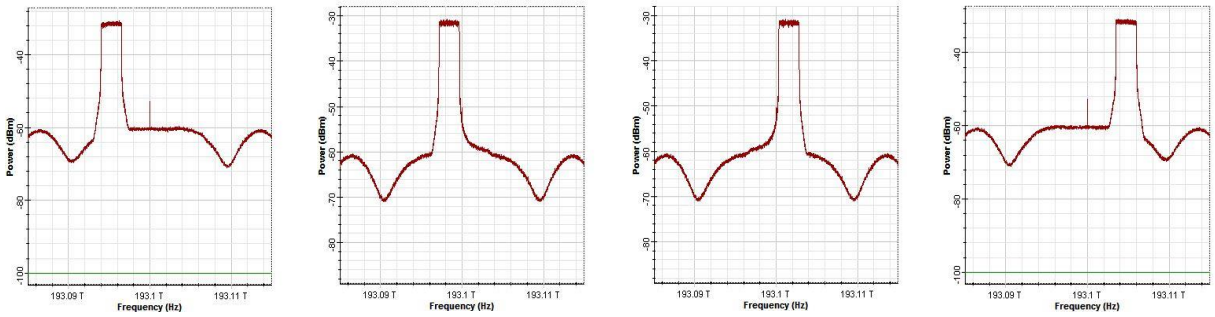

(a) Case one (b) Case two (c) Case three (d) Case four

Figure 4.6: CO OFDM receiving power spectrum

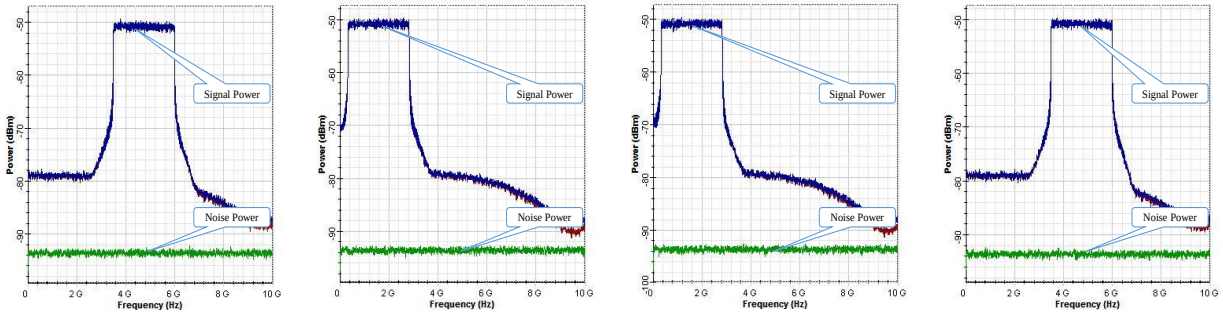

(a) Case one (b) Case two (c) Case three (d) Case four

Figure 4.7: RF-OFDM receiving power spectrum

phase dispersion increases when the frequencies of the 64-subcarriers increase, as in cases one and four. This phase dispersion occurs because of the fiber chromatic and polarization mode dispersion.

In cases one and two, the phase dispersion is equal to the chromatic dispersion plus polarization mode dispersion, while in cases three and four it is equal to polarization mode dispersion subtracted from the chromatic dispersion. Fig 4.8c shows that case three has

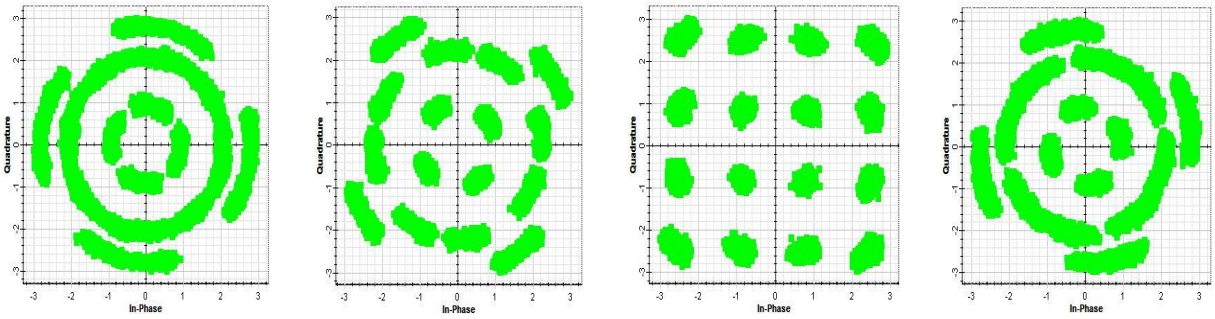

(a) Case one (b) Case two (c) Case three (d) Case four

Figure 4.8: 16-QAM constellation diagram for output of OFDM demodulator

a better constellation diagram because the value of phase dispersion from fiber chromatic dispersion is almost the same as the fiber polarization mode dispersion. Fig 4.9 illustrates the $\log(BER)$ with different locations for the 64 subcarriers. Once again, case three, where the 64 subcarriers span between the 266^{th} and 329^{th}, has the lowest BER.

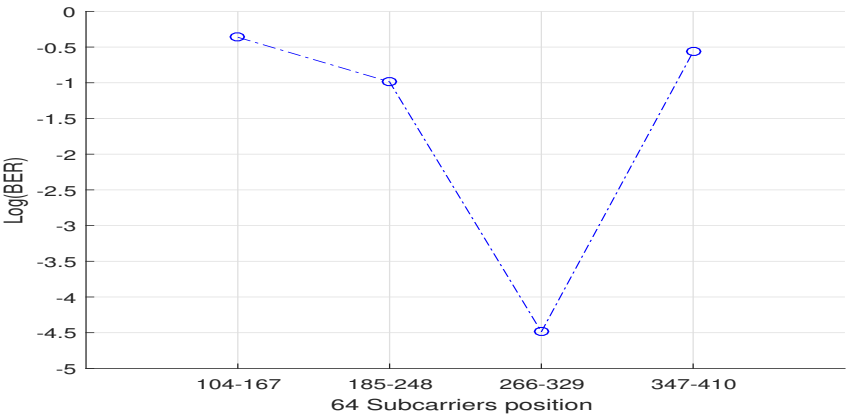

Figure 4.9: The relationship of the $\log(BER)$ and Subcarrier position

4.3 Evaluating the system with phase dispersion compensation

In this section, a simulation test is performed for the same system as above, plus a phase dispersion compensator. In [22], the phase dispersion is defined as in Eq. 4.10, but the authors have considered only the chromatic dispersion component. The research of this thesis, however, has determined that polarization mode dispersion cannot be neglected, and thus another component has been added to the phase dispersion as per Eq. 4.11, thereby eliminating the impact of polarization mode dispersion. Therefore, in the propose model, the phase dispersion is defined as in Eq. 4.12.

$$\phi_{CD}(k) = \frac{\pi c}{f_{LD}^2} D.f_k^2 \tag{4.10}$$

$$\phi_{PMD}(k) = \pm \pi f_k.DGD.L \tag{4.11}$$

$$\phi_D(k) = \phi_{CD}(k) + \phi_{PMD}(k) \tag{4.12}$$

where f_k is the frequency of the subcarrier, and ϕ_{PMD} is negative when the subcarrier is located on the right side of the zero subcarrier frequency.

There are many types of phase dispersion compensation, such as using pilot subcarriers in the OFDM symbol to estimate the phase, but this method reduces the net data rate as per Eq. 4.6. This theses proposes compensating for the phase dispersion by adding

DCF to the optical link, which will eliminate the component of chromatic dispersion, and setting the initial phase in the local oscillator at the coherent receiver to compensate for the polarization mode dispersion. For simplicity, the middle frequency of the 64-subcarrier band is used in Eq. 4.11 as an average frequency for all 64 subcarriers, because the Optisystem simulation tool does not have the capability of accessing each subcarrier in the optical domain. The proposed design evaluated against the pilot technique.

4.3.1 Compensate phase dispersion by using DCF and initial phase shift

In this simulation, a DCF is added in the optical link with an attenuation of $0.4dB/km$, dispersion of $-80ps/nm/km$, and DGD of $0.2ps/km$. The other system parameters are kept the same except that the length of the optical link is divided between SMF and DCF, at ration of 5/6 and 1/6, respectively, and the initial phase of the local oscillator is set as per table 4.2.

Table 4.2: Initial phase for each 64-subcarrier location

64-subcarriers location	Initial phase
$23^{th} - 86^{th}$	23.92
$104^{th} - 167^{th}$	14.35
$185^{th} - 248^{th}$	4.78
$266^{th} - 329^{th}$	-4.78
$347^{th} - 410^{th}$	-14.35
$428^{th} - 491^{st}$	-23.92

Fig. 4.10 shows that, after simulation, the system with a phase dispersion compensator

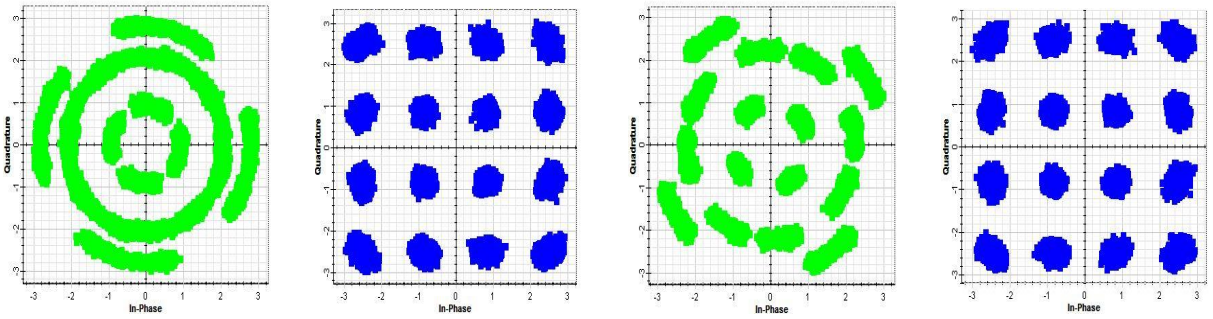

(a) Case one without phase dispersion compensator

(b) Case one with phase dispersion compensator

(c) Case two without phase dispersion compensator

(d) Case two with phase dispersion compensator

(e) Case three without phase dispersion compensator

(f) Case three with phase dispersion compensator

(g) Case four without phase dispersion compensator

(h) Case four with phase dispersion compensator

Figure 4.10: 16-QAM constellation diagram for the designed system with/without phase dispersion compensator

has a better constellation diagram than the system without a phase dispersion compensator, even for the diagram that show higher impact for the phase dispersion. For example, Fig. 4.10a shows high phase dispersion in the constellation diagram for the 64-subcarriers located from 104^{th} to 167^{th}, while Fig. 4.10b shows a clear constellation diagram for the same position of the 64-subcarriers. Fig. 4.11 shows the relation between transmitting

power and the $log(BER)$ for all cases. As can be noticed, the $log(BER)$ decreases when the transmitting power increases. Cases one and four need more power than cases two and three in order to have the same BRE.

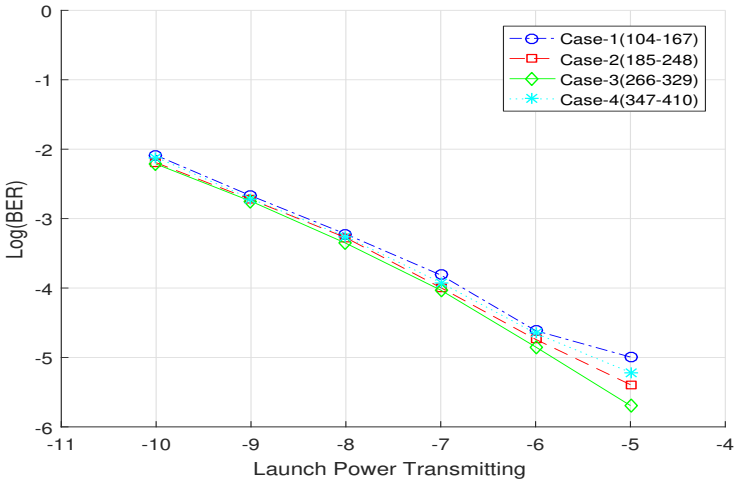

Figure 4.11: The relationship between the BER and transmitting power

4.4 Summary

In this chapter, a single-band of 16QAM CO-OFDM system with a bit rate of $10Gbps$ has been designed and simulated. The simulation results show that the system has low performance at high RF, because non-linear impairments of the optical fiber have higher impact on high RF. After that, the system was modified to compensate for the chromatic dispersion and polarization mode dispersion. Then, a simulation was performed and shows improved system performance even for high RF.

Chapter 5

System Performance of a Multi-band CO-OFDM Based LRPON

Based on the knowlesge gained in the design of a single-band optical OFDM system in the previous chapter, this chapter discusses a multi-band CO-OFDM based LRPONs, which aims to provide high data rate for numerous ONUs and long transmission distance between OLT and ONUs. A simulation is performed using Optisystem. In addition, DCF and LO phase shifter uses to compensate for CD and PMD.

This chapter is organized as follows. It starts with an introduction of the proposed operational architecture for multi-band CO-OFDM LRPON system; then it describes the simulation setup and the results of the proposed system under various digital-modulation formats and transmission lengths.

5.1 Proposed Multi-band CO-OFDM PON Architecture

Fig. 5.1 shows the proposed multi-band CO-OFDM PON architecture, which consists of an optical line terminal (OLT), an optical distribution network (ODN), and multiple optical network units (ONU). In the OLT, the N users' data are coded and mapped to one OFDM modulator with an IFFT size of L points. Each user's data is assigned to a specific location on the IFFT, and has a number of subcarriers N_{sc}^{i} to generate a sub-band OFDM with the bandwidth Bw, where i is the number of users. A guard band GB is needed to avoid ISI and ICI; therefore, null subcarriers are inserted on the IFFT between two adjacent sub-bands' edges, as shown in Fig. 5.2.

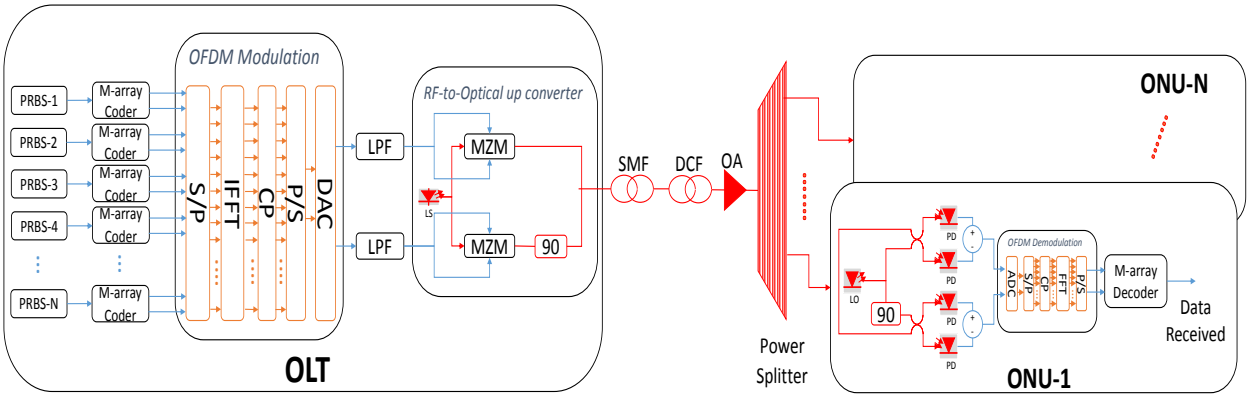

Figure 5.1: Proposed Multi-band CO-OFDM PON Architecture

The IFFT module has a subcarrier called zero subcarrier with zero frequency, and it is

located at $\frac{L}{2}+1$. The remaining subcarriers located from one to $\frac{L}{2}$ are called left subcarriers, and the subcarriers located from $\frac{L}{2}+2$ to L are called right subcarriers. Thus, the IFFT module comes up with two OFDM spectra for the left and right subcarriers, and the spectra have the same frequencies from zero to $\Delta f \times \frac{L}{2}$, where Δf is the subcarrier spacing. After the IFFT, a CP is inserted into the mutli-band OFDM symbol period. Following the P/S converter, DAC, and low pass filter, the in-phase I and quadratic Q components of the multi-band OFDM are up converted to OSSB using two MZMs, and a CW laser with a launch power P. The zero subcarrier is shifted to an optical carrier frequency, while the left and the right subcarriers' frequencies are shifted to the left and the right of the optical carrier frequency. The total multi-band CO-OFDM bandwidth f_{BW} will be twice that of $\Delta f \times \frac{L}{2}$.

In ODN, the multi-band CO-OFDM signal is transmitted over D km SSMF and d km DCF, where DCF is used to compensate for the chromatic dispersion. The multi-band CO-OFDM signal is amplified by an optical amplifier to compensate for fiber attenuation, after that the signal is split among the ONUs by the passive optical splitter, at a ratio $1:N$. In the ONU, a coherent detector is used to down convert optical signals to RF signals. A certain phase shift is applied in the LO laser of the coherent detector to compensate for the polarization mode dispersion. This phase is not the same for all ONUs; it depends on the differential group delay of the fiber, and the frequency difference between an optical

carrier and a sub-band frequency of the ONU in the optical domain.

The RF-down-conversion's output is passed to an OFDM demodulator, which reverse the OFDM modulator's process. It also will select the ONU sub-band according to the assigned locations of ONU's subcarriers on the FFT module. The subcarriers must be synchronized with their assigned locations on the transmission side. Finally, the output sequence from OFDM demodulator is decoded to its original shape.

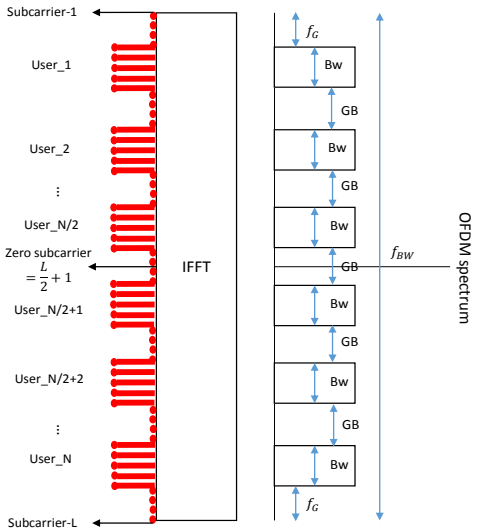

Figure 5.2: Assigning Subcarriers for Multi-band OFDM

5.2 Simulation Setup and result

The proposed multi-band CO-OFDM PON architecture is simulated by an OptiSystem V.14 platform. This simulation tests the downlink performance between one OLT and

12 ONUs. At the OLT, a random binary sequence of $10Gbps$ is generated for each ONU and mapped to an M-array coder, which is either 16QAM or 16PSK. The 12 sequences are modulated into a 12-band OFDM signal by an OFDM modulator with the following parameters: 1024 IFFT points, 64 subcarriers for each sub-band, and located as shown in Table 5.1, and a 1/16 CP ratio.

Table 5.1: The properties of the Sub-bands

ONUs	Subcarriers Location on IFFT	Base-band Frequency (GHz)	Optical Frequency (THz)	LO laser Phase Shift
Subband-1	69:132	16.1133	193.08389	46.41
Subband-2	144:207	13.1836	193.08682	37.97
Subband-3	219:282	10.2539	193.08975	29.53
Subband-4	294:357	7.3242	193.09268	21.09
Subband-5	369:432	4.3945	193.09561	12.66
Subband-6	444:507	1.4648	193.09854	4.22
Subband-7	519:582	1.4648	193.10146	-4.22
Subband-8	594:657	4.3945	193.10439	-12.66
Subband-9	669:732	7.3242	193.10732	-21.09
Subband-10	744:807	10.2539	193.11025	-29.53
Subband-11	819:882	13.1836	193.11318	-37.97
Subband-12	894:957	16.1133	193.11611	-46.41

Column 3 in Table 5.1 shows the base-band central frequencies for all sub-bands. Clearly, the first 6 sub-bands, which are located on the left side of the zero subcarrier, have the same base band central frequencies as the other 6-bands are located on the right side of the zero subcarrier. Two symmetrical 6-band OFDM signals, representing both left and right subcarriers are generated, as shown in Fig. 5.3a and 5.3b, respectively with a

$2.5GHz$ bandwidth for each sub-band, $39.0625MHz$ subcarrier spacing, and a $468.75MHz$ guard band.

The I and Q components of the OFDM modulator are passed into two MZMs with a CW laser at a frequency $193.1THz$ and launching power of -$5dBm$ to generate an OSSB for both 6-band OFDM signals. Fig. 5.3c shows the 12-band CO-OFDM spectrum, with 6-bands on the left side of the optical carrier ($193THz$), and the other 6-bands on the right side. The optical signal was transmitted over a total fiber length of $80km$, where $66.66km$ is the type of SSMF with an attenuation of $0.2dBm/km$, a dispersion of $16ps/nm/km$, and a differential group delay (DGD) of $0.2ps/km$, and $13.34km$ is the type of DCF with an attenuation of $0.4dBm/km$, a dispersion of -$80ps/nm/km$, and a DGD of $0.2ps/km$. Following the optical amplifier with a gain of $18.6dB$, a passive power splitter was used to split the optical signal on the 12 ONUs.

At each ONU, the signal is coherently detected by a four PIN and LO laser with a frequency of $193.1THz$ and phase shift as shown in Table 5.1. After that, the OFDM demodulator digitally selects the sub-band that belongs to the ONU, by assigning the locations of subcarriers in the OFDM demodulator to be the same as the subcarriers' locations in the OFDM modulator, as originally assigned to this ONU. Finally, the BER is measured to evaluate the performance of the proposed architecture, and compared with the BERs' of two other architectures: conventional OFDM, where no DCF and phase shift

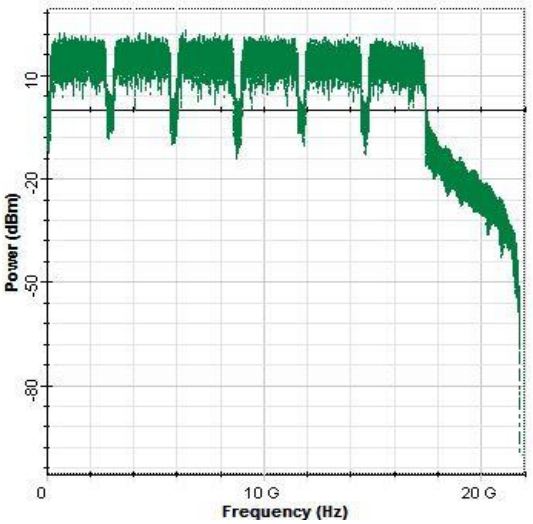

(a) 6-bands OFDM spectrum represents for the left subcarriers

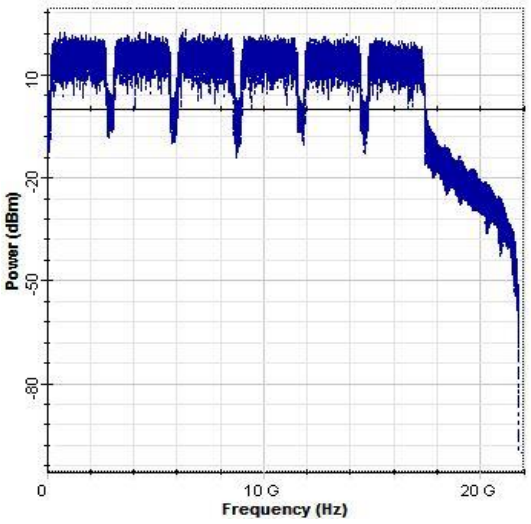

(b) 6-bands OFDM spectrum represents for the right subcarriers

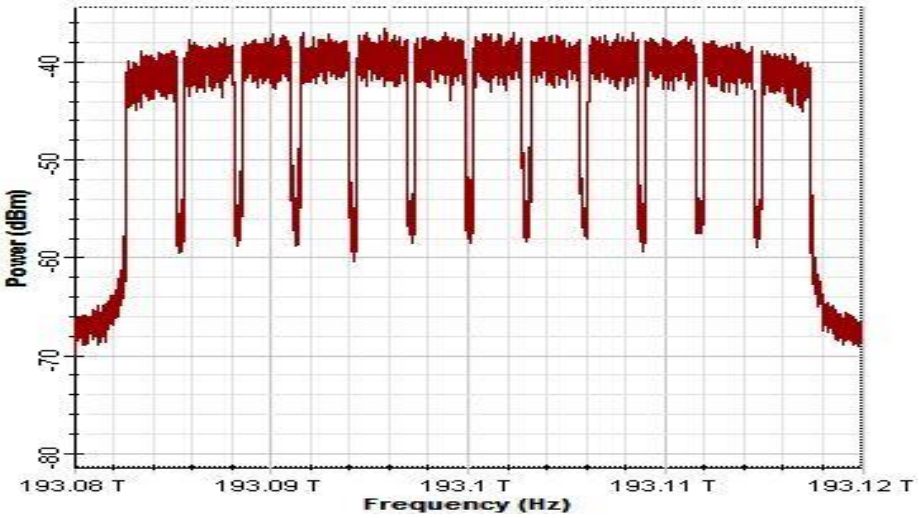

(c) 12-bands CO-OFDM spectrum represents for both the left and the right subcarriers

Figure 5.3: Multi-band OFDM spectrum

are implemented, and conventional OFDM plus DCF, where only DCF is used. In Fig. 5.4, the proposed multi-band CO-OFDM architecture, for both 16QAM and 16PSK shows a lower BER than those of the other two architectures, even when the sub-band has a high frequency such as ONU-1, ONU-2, ONU-11, and ONU-12. In addition, the 16QAM shows better performance than 16PSK for all ONUs except for ONU-1 and ONU12, which they have the highest base band frequency of $16.11GHz$.

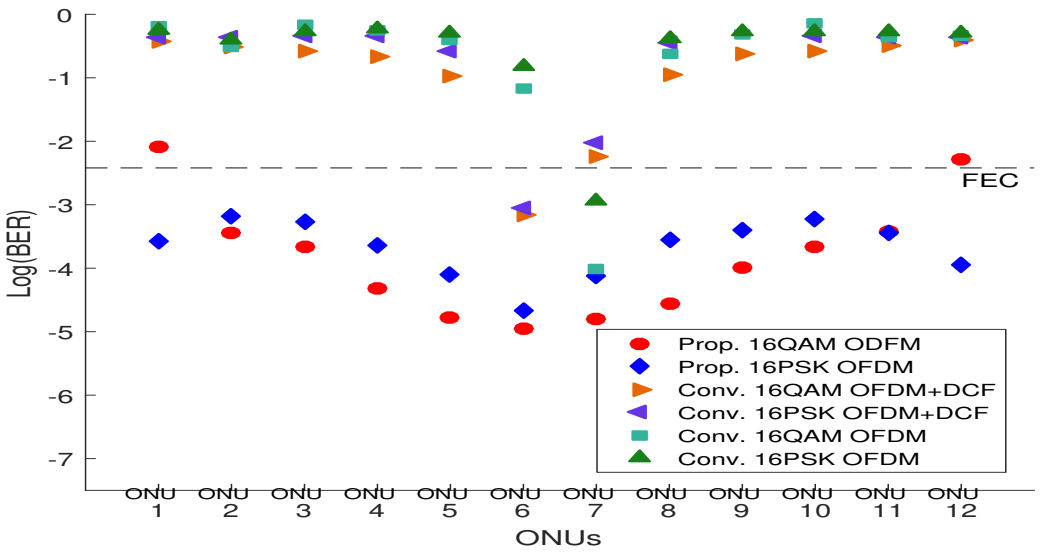

Figure 5.4: Measured BER for the proposed multi-band CO-OFDM PON architecture compared with conventional CO-OFDM

Fig. 5.5 illustrates the 16QAM and 16PSK constellations diagram for some ONUs at the conventional CO-OFDM, conventional CO-OFDM plus DCF, and proposed CO-OFDM architectures. It is clearly shown that the high sub-band's frequency cannot be used in

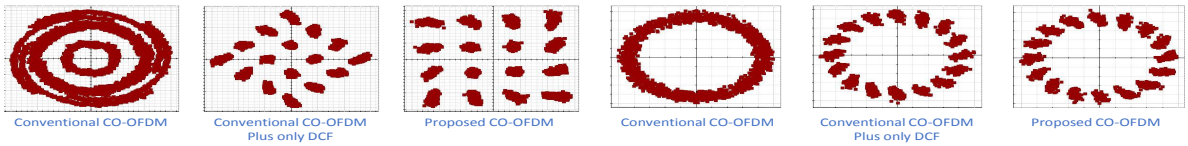

(a) 16QAM Sub-band 1 (b) 16PSK Sub-band 1

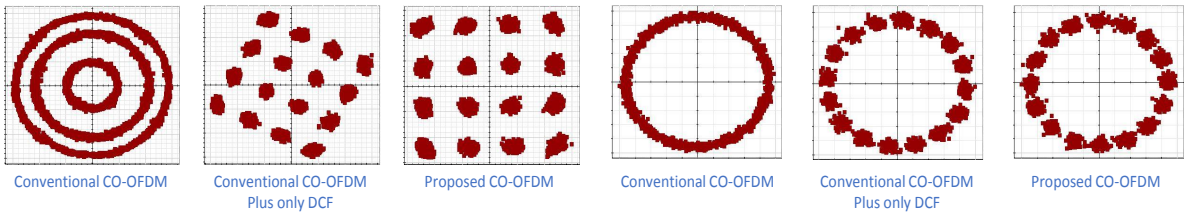

(c) 16QAM Sub-band 3 (d) 16PSK Sub-band 3

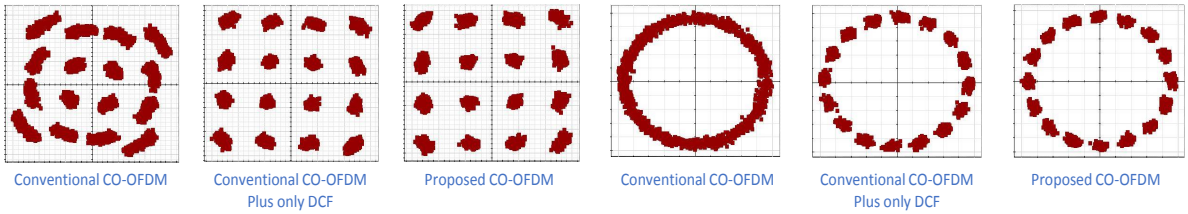

(e) 16QAM Sub-band 6 (f) 16PSK Sub-band 6

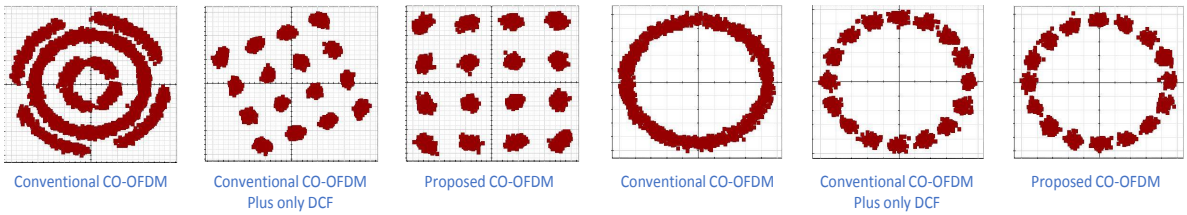

(g) 16QAM Sub-band 9 (h) 16PSK Sub-band 9

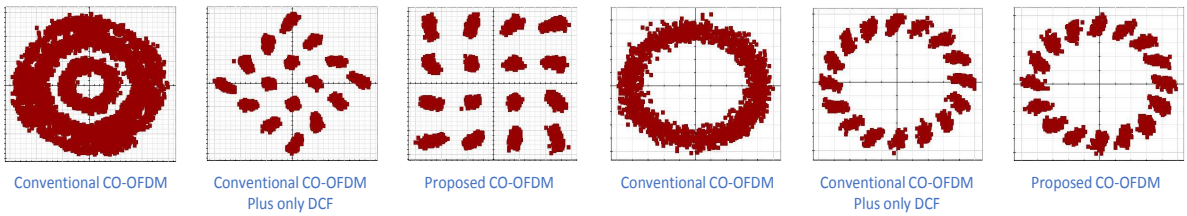

(i) 16QAM Sub-band 12 (j) 16PSK Sub-band 12

Figure 5.5: 16QAM and 16PSK constellation diagram for some sub-bands

conventional CO-OFDM, because of the chromatic and polarization mode dispersions. Even though the chromatic dispersion is eliminated by DCF in conventional CO-OFDM plus DCF, which shows more improvement for the constellation than conventional one, the DGD still creates a phase shift, and the phase is increased at the higher frequencies. In contrast,The proposed CO-OFDM architecture, where the DCF and LO laser phase shift has been implemented, has the clearest constellation diagram, even for higher frequencies, such as sub-band 1, sub-band 3, sub-band 9, and sub-band 12 in Fig. 5.5a, 5.5c, 5.5g, and 5.5i for 16QAM respectively, and sub-band 1, sub-band 3, sub-band 9, and sub-band 12 in Fig. 5.5b, 5.5d, 5.5h, and 5.5j for 16PSK, respectively.

Simulation result with CW launched power of -6 dBm

Fig. 5.6 shows the measurements of BER for 16QAM and 16PSK multi-band CO-OFDM, respectively, with -6dBm CW transmission power at fiber lengths of 70, 80, 90, and 100km, respectively. The results show that the ONU-1 and ONU-12, which have a baseband frequency of 16.11GHz, could not achieve the minimum BER (3.8×10^{-3}) for required forward error correction (FEC) under 16QAM, whereas ONU-(2, 3, 10, and 11) could not achieve the minimum BER under a transmission length of over 90s km. ONU-(4, 5, 6, 7, 8, and 9) did achieve the minimum BER under all considered transmission lengths, as demonstrated in Fig. 5.6a. In contrast, the 16PSK shows that almost all ONUs have

achieved the minimum BER under all considered transmission fiber lengths, except ONU-(3 and 10) which manage to achieve the minimum BER for the transmission length up to 95 km

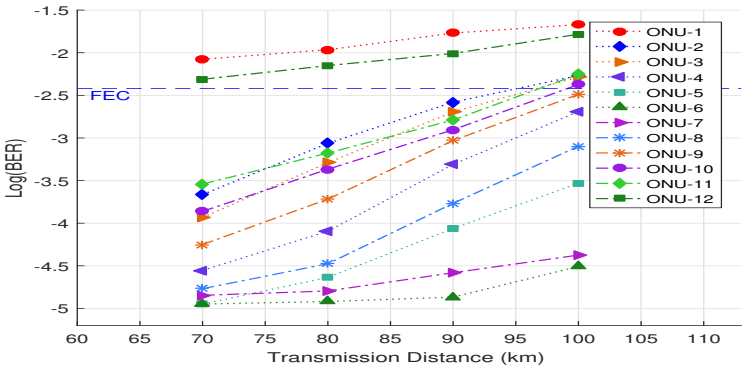

(a) 16QAM 1

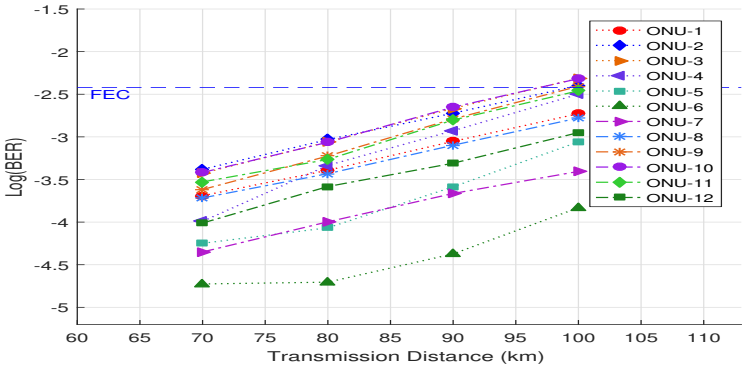

(b) 16PSK 1

Figure 5.6: The BRE at CW laser launched power -6dBm against transmission fiber length

Simulation result with CW launched power of -2 dBm

The system's performance is improved by increasing the CW launched power to -2 dBm. Fig. 5.7a shows the result of 16QAM, where the BER of all ONUs are bellow the BER

threshold (3.8×10^{-3}) under all considered transmission fiber lengths. Furthermore, the 16PSK shows that also all ONUs achieve the minimum BER that required for FEC under all considered transmission fiber lengths, as shown in Fig. 5.7b.

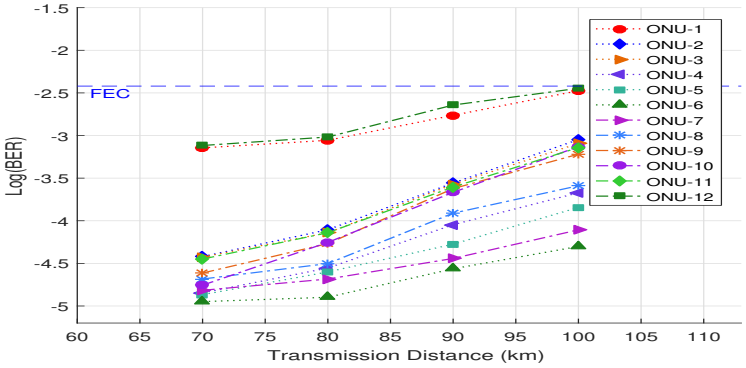

(a) 16QAM 1

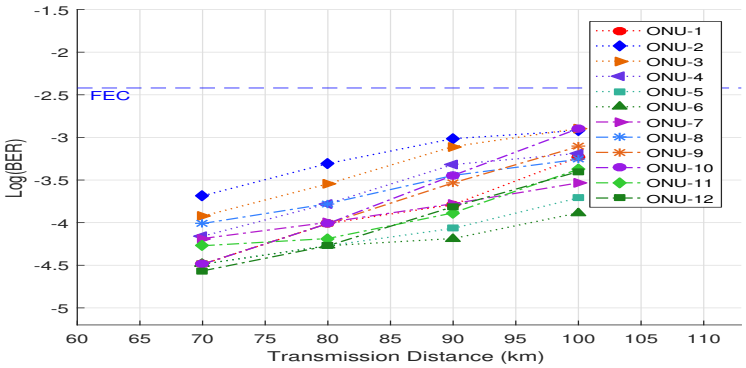

(b) 16PSK 1

Figure 5.7: The BRE at CW laser launched power -2dBm against transmission fiber length

5.3 Summary

This chapter has demonstrated a successful design for a multi-band CO-OFDM PON architecture through simulation with a high data rate per user, long distance, and multiple users. The DCF and LO phase shift were implemented to compensate for the dispersion components in order to improve ONU performance quality. The proposed architecture has been simulated to transmit $120Gbps$ between one OLT and 12 ONUs at different fiber lengths. For concept validation, the architecture has been tested using two modulation techniques (16QAM and 16PSK). Results show that the 16QAM multi-band CO-OFDM has the potential to support up to 10 OUNs, with a data rate of $10Gbps$ for each one, and a fiber length of $100km$. In contrast, the 16PSK multi-band CO-OFDM can support up to 12 ONUs with the same data rate and a fiber length of up to $90km$. However, the complexity of the architecture is increased using DCF, but the overhead data does not increase as much as when using training-symbol and pilot-subcarrier techniques.

Chapter 6

Conclusion and Future Work

6.1 Conclusions

The thesis has studied an optical coherent orthogonal frequency division multiplexing (CO-OFDM), which is one of the candidates for long reach passive optical network (LRPON) due to its spectral efficiency and cost effectiveness. This thesis has investigated the CO-OFDM in two stages as follows

Chapter 4 has designed and simulated a single-band of a 16QAM CO-OFDM system with a bit rate of $10Gbps$. The simulation results show that the system has low performance at high RF, because non-linear impairments of the optical fiber have a higher impact on high RF. After that, the system was modified to compensate for the chromatic dispersion and polarization mode dispersion. Then, a simulation was performed and shows improved system performance even for high RF.

Chapter 5 has demonstrated a successful design for a multi-band CO-OFDM LRPON architecture through simulation with a high data rate per user, long distance, and multiple users. The DCF and LO phase shift were implemented to compensate for the dispersion components in order to improve ONU performance quality. The proposed CO-OFDM LRPON architecture was simulated using Optiwave, and the results demonstrate that the legacy problem of chromatic and polarization dispersions in CO-OFDM LRPON can be effectively resolved. However the complexity of the architecture is increased due to the DCF, even though the overhead data does not increase as much as when using training-symbol and pilot-subcarrier techniques.

6.2 Future Work

The future research topics of the thesis will be listed as follows.

- Consider the dynamic bandwidth allocation when assigning the subcarriers in order to increase spectrum efficiency.
- Examine how to reduce the guard band between sub-band OFDM without decreasing system performance, thus increasing spectrum efficiency.
- Investigate how to compensate for the chromatic dispersion without using DCF, and so reduce the system's budget.

- Investigate ways to optimize the launched power.

References

[1] J. Armstrong, "Ofdm for optical communications," *Lightwave Technology, Journal of*, vol. 27, no. 3, pp. 189–204, 2009.

[2] Y. Tang and W. Shieh, "Coherent optical ofdm transmission up to 1 tb/s per channel," *Journal of lightwave technology*, vol. 27, no. 16, pp. 3511–3517, 2009.

[3] W. Zhou and J. Ma, "A novel multi-band ofdma-pon architecture using signal-to-signal beat interference cancellation receivers based on balanced detection," *Photonic Network Communications*, pp. 1–7, 2015.

[4] I. N. Cano, X. Escayola, P. C. Schindler, M. C. Santos, V. Polo, J. Leuthold, I. Tomkos, and J. Prat, "Experimental demonstration of a statistical ofdm-pon with multiband onus and elastic bandwidth allocation [invited]," *Journal of Optical Communications and Networking*, vol. 7, no. 1, pp. A73–A79, 2015.

[5] I. Cano, X. Escayola, P. Schindler, M. C. Santos, V. Polo, J. Leuthold, and J. Prat, "Experimental demonstration of multi-band upstream in statistical ofdm-pons and comparison with digital subcarrier assignment," in *Optical Fiber Communication Conference*. Optical Society of America, 2014, pp. Th3G–4.

[6] N. Cvijetic, M. Cvijetic, M.-F. Huang, E. Ip, Y.-K. Huang, and T. Wang, "Terabit optical access networks based on wdm-ofdma-pon," *Lightwave Technology, Journal of*, vol. 30, no. 4, pp. 493–503, 2012.

[7] N. Cvijetic, M.-F. Huang, E. Ip, Y.-K. Huang, D. Qian, and T. Wang, "1.2 tb/s symmetric wdm-ofdma-pon over 90km straight ssmf and 1: 32 passive split with digitally-selective onus and coherent receiver olt," in *Optical Fiber Communication Conference*. Optical Society of America, 2011, p. PDPD7.

[8] W. Ji, X. Li, Z. Kang, and X. Xue, "Design of wdm-rof-pon based on improved ofdm mechanism and optical coherent technology," *Journal of Optical Communications and Networking*, vol. 7, no. 2, pp. 74–82, 2015.

[9] C.-H. Yeh, C.-W. Chow, and H.-Y. Chen, "Adaptive 6.25-40 gb/s downstream rate using four-band ofdm channels within 10 ghz bandwidth for long-reach pon," in *Optical Fiber Communication Conference*. Optical Society of America, 2012,

p. JTh2A.51. [Online]. Available: http://www.osapublishing.org/abstract.cfm?URI=OFC-2012-JTh2A.51

[10] B. A. Graham, "Improvement in telegraphy," Mar. 7 1876, uS Patent 174,465.

[11] R. W. Chang, "Synthesis of band-limited orthogonal signals for multichannel data transmission," *Bell System Technical Journal*, vol. 45, no. 10, pp. 1775–1796, 1966.

[12] J. Salz and S. Weinstein, "Fourier transform communication system," in *Proceedings of the first ACM symposium on Problems in the optimization of data communications systems*. ACM, 1969, pp. 99–128.

[13] A. Peled and A. Ruiz, "Frequency domain data transmission using reduced computational complexity algorithms," in *Acoustics, Speech, and Signal Processing, IEEE International Conference on ICASSP'80.*, vol. 5. IEEE, 1980, pp. 964–967.

[14] L. J. Cimini Jr, "Analysis and simulation of a digital mobile channel using orthogonal frequency division multiplexing," *Communications, IEEE Transactions on*, vol. 33, no. 7, pp. 665–675, 1985.

[15] R. Lassalle and M. Alard, "Principles of modulation and channel coding for digital broadcasting for mobile receivers," *EBU Tech. Rev*, vol. 224, pp. 168–190, 1987.

[16] J. S. Chow, J. C. Tu, and J. M. Cioffi, "A discrete multitone transceiver system for hdsl applications," *Selected Areas in Communications, IEEE Journal on*, vol. 9, no. 6, pp. 895–908, 1991.

[17] O. González, R. Pérez-Jiménez, S. Rodriguez, J. Rabadán, and A. Ayala, "Ofdm over indoor wireless optical channel," in *Optoelectronics, IEE Proceedings-*, vol. 152, no. 4. IET, 2005, pp. 199–204.

[18] J. Grubor, V. Jungnickel, and K.-D. Langer, "Adaptive optical wireless ofdm system with controlled asymmetric clipping," in *Signals, Systems and Computers, 2007. ACSSC 2007. Conference Record of the Forty-First Asilomar Conference on.* IEEE, 2007, pp. 1896–1902.

[19] B. J. Schmidt, A. J. Lowery, and J. Armstrong, "Experimental demonstrations of electronic dispersion compensation for long-haul transmission using direct-detection optical ofdm," *Journal of Lightwave Technology*, vol. 26, no. 1, pp. 196–203, 2008.

[20] Q. Yang, A. Al Amin, and W. Shieh, "Optical ofdm basics," in *Impact of Nonlinearities on Fiber Optic Communications.* Springer, 2011, pp. 43–85.

[21] J. G. Proakis and D. G. Manolakis, *Digital Signal Processing (3rd Ed.): Principles, Algorithms, and Applications.* Upper Saddle River, NJ, USA: Prentice-Hall, Inc., 1996.

[22] W. Shieh and C. Athaudage, "Coherent optical orthogonal frequency division multiplexing," *Electronics letters*, vol. 42, no. 10, p. 1, 2006.

[23] I. Shieh, William. Djordjevic, *OFDM for Optical Communications*. San Diago, CA, USA: Academic Press, 2010.

[24] W. Shieh, H. Bao, and Y. Tang, "Coherent optical ofdm: theory and design," *Optics express*, vol. 16, no. 2, pp. 841–859, 2008.

[25] W. Wang, R. Tavlykaev, and R. V. Ramaswamy, "Bandpass traveling-wave mach-zehnder modulator in linbo3 with domain reversal," *IEEE Photonics Technology Letters*, vol. 9, no. 5, pp. 610–612, May 1997.

[26] A. Enokihara, H. Yajima, H. Murata, and Y. Okamura, "Electro-optic intensity modulator using higher-order resonant electrode with polarization-reversed structure," in *2005 European Microwave Conference*, vol. 1, Oct 2005, pp. 4 pp.–.

[27] X. Li, R. Mardling, and J. Armstrong, "Channel capacity of im/dd optical communication systems and of aco-ofdm," in *2007 IEEE International Conference on Communications*, June 2007, pp. 2128–2133.

[28] Liu, Wanzong, "The end-to-end ber analysis of two simulated ofdm-rof systems," 2016. [Online]. Available: https://uwspace.uwaterloo.ca/handle/10012/10100

[29] ITU-T, "40-gigabit-capable passive optical networks (ng-pon2): General requirements," Digital sections and digital line system Optical line systems for local and access networks, Recommendation G.989.1, 2013.

[30] Y.-W. Chen, J.-H. Yan, Y.-M. Wang, M.-F. Chang, W.-R. Peng, and K.-M. Feng, "Over 210 gb/s pdm multiband ddo-ofdm lr-pon downstream with simple self-polarization diversity," *Optics express*, vol. 23, no. 14, pp. 18 525–18 533, 2015.

[31] P. Ossieur, C. Antony, A. M. Clarke, A. Naughton, H.-G. Krimmel, Y. F. Chang, C. Ford, A. Borghesani, D. Moodie, A. Poustie *et al.*, "A 135-km 8192-split carrier distributed dwdm-tdma pon with 2 32 10 gb/s capacity," *Lightwave Technology, Journal of*, vol. 29, no. 4, pp. 463–474, 2011.

[32] O. González, R. Pérez-Jiménez, S. Rodrıguez, J. Rabadán, and A. Ayala, "Adaptive ofdm system for communications over the indoor wireless optical channel," *IEE Proceedings-Optoelectronics*, vol. 153, no. 4, pp. 139–144, 2006.